ARTICLE

Tumor suppression of novel anti–PD-1 antibodies mediated through CD28 costimulatory pathway

Craig Fenwick[1], Juan-Luis Loredo-Varela[3]*, Victor Joo[1]*, Céline Pellaton[1], Alex Farina[1], Navina Rajah[1], Line Esteves-Leuenberger[1], Thibaut Decaillon[1], Madeleine Suffiotti[1], Alessandra Noto[1], Khalid Ohmiti[1], Raphael Gottardo[4], Winfried Weissenhorn[3], and Giuseppe Pantaleo[1,2]

Classical antagonistic antibodies (Abs) targeting PD-1, such as pembrolizumab and nivolumab, act through blockade of the PD-1–PDL-1 interaction. Here, we have identified novel antagonistic anti–PD-1 Abs not blocking the PD-1–PDL-1 interaction. The nonblocking Abs recognize epitopes on PD-1 located on the opposing face of the PDL-1 interaction and overlap with a newly identified evolutionarily conserved patch. These nonblocking Abs act predominantly through the CD28 coreceptor. Importantly, a combination of blocking and nonblocking Abs synergize in the functional recovery of antigen-specific exhausted CD8 T cells. Interestingly, nonblocking anti–PD-1 Abs have equivalent antitumor activity compared with blocker Abs in two mouse tumor models, and combination therapy using both classes of Abs enhanced tumor suppression in the mouse immunogenic tumor model. The identification of the novel nonblocker anti–PD-1 Abs and their synergy with classical blocker Abs may be instrumental in potentiating immunotherapy strategies and antitumor activity.

Introduction

The programmed cell death 1 receptor (PD-1) is the master regulator of T cells through the suppression of T cell activation following the binding to its primary ligand, programmed death ligand 1 (PDL-1; Trautmann et al., 2006; Tumeh et al., 2014; Pauken and Wherry, 2015; Wherry and Kurachi, 2015). The proposed mechanism by which PD-1 acts as an immune checkpoint inhibitor includes recruitment of the SHP-2 phosphatase into the vicinity of the TCR complex, resulting in dephosphorylation of membrane proximal signaling proteins, including CD3ζ, ZAP70, and PLC-γ1 (Sheppard et al., 2004; Yokosuka et al., 2012). The PD-1–SHP-2 complex also acts on the CD28 costimulatory receptor and the associated PI3K and AKT signaling pathway needed for optimal T cell activation and survival (Parry et al., 2005; Patsoukis et al., 2012). These dynamics have been observed in fluorescence microscopy imaging studies where PD-1 exists in microclusters on the cell surface and is recruited along with SHP-2 phosphatase into the immunological synapse to suppress phosphorylation events during TCR activation (Chemnitz et al., 2004; Sheppard et al., 2004; Yokosuka et al., 2012; Wherry and Kurachi, 2015). Two recent studies have also indicated that anti–PD-1–mediated tumor-suppressive activity is primarily dependent of the CD28 costimulatory receptor (Hui et al., 2017; Kamphorst et al., 2017).

Monoclonal antibodies (Abs) acting through PD-1 blockade represent a major breakthrough in oncology, showing significant clinical success in the treatment of several types of cancer, including advanced melanoma, non–small cell lung cancer, and head and neck squamous cell carcinoma (Baitsch et al., 2011; Mellman et al., 2011; Topalian et al., 2012; Hamid et al., 2013; Rizvi et al., 2015; Sharma and Allison, 2015; Callahan et al., 2016). Despite these successes, only ∼30–40% of patients show a response to anti–PD-1 immunotherapy, and only a fraction of these show a durable clinical response. These limitations highlight the need for a better understanding of the mechanism by which anti–PD-1 Abs act and for the identification of new therapies that synergize to improve the response rate and/or breadth of cancers that can be treated.

The objective of the present study was to identify novel antagonist Abs with more potent antitumor activity and/or acting through a mechanism independent of the PD-1–PDL-1 blockade. A panel of Ab clones binding with high affinity to diverse epitopes on PD-1 was generated and profiled for antagonistic activity in recovering antigen (Ag)–specific CD8 T cells from functional exhaustion. A novel class of anti–PD-1 Ab was identified that was not blocking the PD-1–PDL-1 interaction with antagonistic activity comparable to pembrolizumab and nivolumab. Antagonistic activity of the novel

[1]Service of Immunology and Allergy, Department of Medicine, Lausanne University Hospital, University of Lausanne, Lausanne, Switzerland; [2]Swiss Vaccine Research Institute, Lausanne University Hospital, University of Lausanne, Lausanne, Switzerland; [3]University Grenoble Alpes, Commissariat à l'Energie Atomique, Centre National de la Recherche Scientifique, Institut de Biologie Structurale, Grenoble, France; [4]Division of Public Health Sciences, Fred Hutchinson Cancer Research Center, Seattle, WA.

*J.-L. Loredo-Varela and V. Joo contributed equally to this paper; Correspondence to Giuseppe Pantaleo: giuseppe.pantaleo@chuv.ch.

anti–PD-1 Abs was determined by evaluating their ability to recover proliferation and/or to potentiate cytokine production of exhausted Ag-specific CD8 T cells. Biochemical and structural studies demonstrated that these Abs bound to the opposite face of the PD-1 protein relative to the PD-1–PDL-1 interaction site. In mechanistic studies, nonblocking anti–PD-1 Abs act predominantly through the CD28 coreceptor that restores signaling through the AKT–NF-κB pathway and leads to T cell proliferation and survival. Consisted with nonblocking anti–PD-1 Abs acting through a distinct mechanism of action, combinations of nonblocking and blocking anti–PD-1 Abs synergize to recover the functional activity of exhausted Ag-specific CD8 T cell in vitro and resulted in significantly enhanced antitumor activity in the MC38 immunogenic in vivo mouse tumor model.

Results

Characterization of a diverse panel of anti–PD-1 Abs binding different epitopes on PD-1

An immunization campaign with human PD-1 was launched in mice, and over 2,000 hybridoma clones were generated and screened in a Luminex assay for binding to recombinant human PD-1. Forty different Ab families with subnanomolar affinity were selected based on (1) possessing low nanomolar binding affinity for cell-surface PD-1, (2) competitive binding profile with a commercially available anti–PD-1 Ab that acted as a surrogate assay to identify blocking Abs of the PD-1–PDL-1 interaction, and (3) heavy-chain complementarity-determining region (CDR) variable region. Anti–PD-1 Abs were further screening to assess both the ability to block the PD-1–PDL-1 interaction in a Luminex biochemical assay and recover Ag-specific CD8 T cells from functional exhaustion. Therefore, the simultaneous use of a functional assay allowed also for the selection of anti–PD-1 Abs with antagonistic activity independent of PD-1–PDL-1 blockade.

The antagonistic, immune-enhancing activity of the novel anti–PD-1 Abs was evaluated in a highly standardized CFSE proliferation assay measuring the recovery of Ag-specific proliferation in blood mononuclear cells from chronically infected viremic HIV patients. HIV-specific CD8 T cells are instrumental to evaluate the ability of anti–PD-1 Abs to recover T cells from functional exhaustion because of the expression of high levels of PD-1 and poor proliferation in response to Ag-specific stimulation (Barber et al., 2006; Day et al., 2006; Trautmann et al., 2006; Zhang et al., 2007). Stimulation of blood mononuclear cells with HIV-derived peptides followed by 6 d in culture led to an increase in CFSE-low CD8 T cells that have undergone proliferation. However, the addition of two classical PDL-1–blocking anti–PD-1 Abs (e.g., pembrolizumab or nivolumab) led to an enhanced level of proliferation relative to the peptide alone control, thus indicating that both anti–PD-1 Abs recover CD8 T cells from exhaustion (Fig. 1, A and B). Validation studies have shown that proliferating CD8 T cells following pembrolizumab treatment were HIV specific, as indicated by pentamer MHC–HIV peptide complex staining. On the basis of the functional activity in this proliferation assay, 10 novel anti–PD-1 Abs showed potency similar to a pembrolizumab, which has been

used as a benchmark control (Fig. 1 B). Anti–PD-1 Ab clones of interest had antagonistic activity that was also replicated using blood mononuclear cells from five different HIV-infected donors having CD8 T cells specific to seven different HIV-derived peptides (Fig. 1, A and B; and Figs. S1 and S2).

We then investigated whether the newly identified antagonistic anti–PD-1 Abs act through PD-1–PDL-1 blockade, as with pembrolizumab and nivolumab. Initial profiling in an Ab competitive binding assay was consistent with two clones binding to a different epitope than the PDL-1 blocking Abs. A Luminex biochemical protein–protein interaction assay was established to test the novel Abs and directly determine PDL-1 binding to a preformed Ab–PD-1 complex. The 135C12 and 136B4 immune-enhancing anti–PD-1 Abs with distinct heavy- and light-chain CDR regions induced only a minor 1.5- to 3-fold reduced affinity of the PDL-1 protein for PD-1 (Fig. 2 A). In contrast, 137F2, which bound competitively to PD-1 with a blocking anti–PD-1 Ab, completely prevented binding of PDL-1 to PD-1–coated beads at all concentrations tested. It is important to underscore that out of the 156 Ab clones with high affinity for PD-1, only 3.2% corresponded to nonblocking Abs with antagonistic activity. The remaining Abs with antagonistic activity (Fig. 1 B) were tested in a PD-1–PDL-1 protein interaction screening assay, and all blocked the PD-1–PDL-1 interaction (Fig. 2 B).

The PD-1–PDL-1 blockade and the CFSE assay results clearly indicate that 135C12 and 136B4 represent novel anti–PD-1 Abs that may exert antagonistic activity independent of blockade of the PD-1–PDL-1 interaction. For these reasons, the two novel nonblocking anti–PD-1 Abs were advanced for more in-depth profiling along with 137F2 blocking Ab, which displayed an improved immune-enhancing activity in our in vitro functional assay relative to pembrolizumab. The CDR sequences for the 135C12 and 137F2 mouse IgG1 Abs were also transferred into a human IgG4 Ab with a panel of constant region clones screened to identify humanized Abs with subnanomolar affinity for cell-surface PD-1. These humanized clones were renamed NB01 for the nonblocking 135C12 Ab and B01 for the blocking 137F2 Ab.

Binding epitopes of antagonistic anti–PD-1 Abs that do not block the PD-1–PDL-1 interaction

Binding epitopes for the three prioritized Abs were then mapped by monitoring binding to a panel of PD-1 proteins expressed with amino acid substitutions at solvent accessible residues of the extracellular domain (Fig. S3 A). Transiently transfected HeLa cells expressed mutant or wild-type forms of PD-1 and allowed for comparative Ab binding to cell-surface PD-1 by flow cytometry (Fig. 2 C). Discrete amino acid substitutions in PD-1 resulted in a loss in binding for selected Abs. Pembrolizumab and 137F2 Abs both mapped to regions previously identified as being important for PDL-1 binding to PD-1 (Lázár-Molnár et al., 2008; Lin et al., 2008), but binding of nonblocking antagonistic Abs was unaffected by these substitutions. 135C12 and 136B4 Ab binding was almost completely disrupted with either M18 (L41A/V43T/S137A/L138A/R139T substitutions) or M32 (D105A substitution) PD-1 constructs, respectively, which are situated on the opposite face to the PD-1 interaction with either PDL-1 or PDL-2. As a
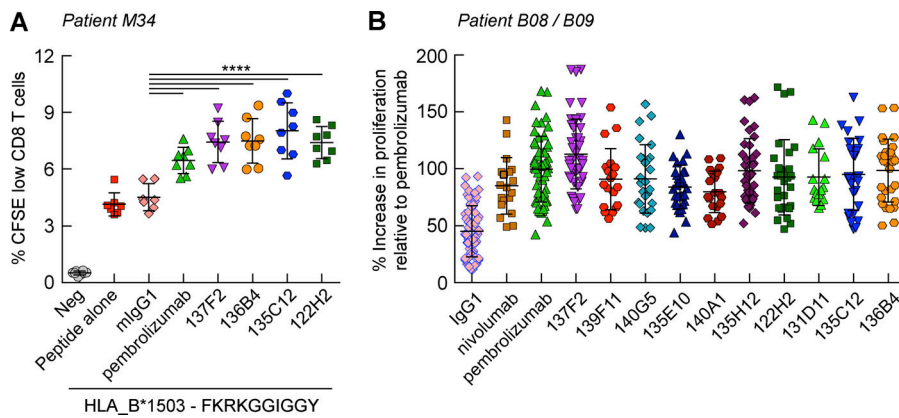
Figure 1. **Anti–PD-1 Abs significantly enhance proliferation of Ag-specific exhausted CD8 T cells. (A)** Recovery of proliferation in HIV-specific CD8 T cells following stimulation with an HIV-derived peptide. Results from a representative experiment are shown and expressed as the percentage of CFSE-low CD8 T cells. 8–10 replicates were performed for each experimental condition. **(B)** Cumulative results from multiple CFSE experiments (n = 2–6) are shown for the 10 anti–PD-1 Abs identified with antagonistic properties similar to pembrolizumab. Results have been generated assessing the proliferation of CD8 T cells specific to three HIV-derived peptides (FLGKIWPSYK restricted by A*0201 and RLRPGGKKK or RMRGAHTNDVK restricted by A*0301) in patients B08 and B09. For comparative purposes across multiple assays and the different anti–PD-1 Abs, the level of proliferation in the pembrolizumab-treated samples was set as a 100% reference. Pembrolizumab was used as a positive control, while untreated (Neg) or mouse IgG1 isotype control Ab was used as a negative control in each experiment. Graphs show the mean ± SD. ****, $P < 0.0001$ for all anti–PD-1 Abs relative to the IgG1 control (unpaired t test with Welch's correction).

further evaluation of Ab-binding characteristics, competitive binding studies were performed with a PD-1–expressing Jurkat cell line. Saturating the PD-1 receptor with the 137F2 blocking Ab prevented cell staining with pembrolizumab, nivolumab, and B01 (humanized 137F2) but did not prevent staining with NB01 (humanized 135C12). Conversely, cell-surface PD-1 saturated with either 135C12 or 136B4 nonblocking Abs had no impact on the binding of pembrolizumab, nivolumab, or B01 Abs to PD-1. Both 135C12 and 136B4 Abs prevented the binding of NB01, the humanized version of the mouse 135C12 Ab (Fig. 2 D), indicating that these Abs bind overlapping epitopes on PD-1. These studies show that antagonistic blocking and nonblocking Abs of the PD-1–PDL-1 interaction can bind to cell-surface PD-1 simultaneously.

To complete the molecular details of the binding epitope of the newly generated PDL-1 nonblocker Abs, the structure of the NB01a (135C12) Fab in complex with hPD-1 was solved at a resolution of 2.2 Å (Table S1). The NB01a Fab binds at the opposite side of the PDL-1–binding site (Fig. 2 E) with interacting residues on PD-1 confirming our mapping studies performed with the 135C12 Ab. The overall structure of hPD-1 fits previously published structures (Zak et al., 2015). Superposition of the Cα atoms of hPD-1 in complex with the NB01a Fab and hPD-1 in complex with hPDL-1 (Protein Data Bank [PDB] accession no. 4ZQK) showed no overlap of the binding footprints for NB01a and hPDL-1, indicating that they can bind PD-1 simultaneously (Fig. 2 E). One potential clash was noted between the hPDL-1 side chains E60/D61 and V_L residues S52/S65 of NB01a; however, these side chains may adopt different rotamers in solution, thereby allowing concomitant binding of hPDL-1 and NB01a to hPD-1. Consequently, the affinity of PDL-1 for hPD-1 in the presence of 135C12/NB01 may be slightly reduced, as observed in the biochemical binding data (Fig. 2 A). It was important to determine whether the four predicted N-glycosylation sites on PD-1 were interfering with NB01 Ab binding. However, the modeling of these sites shows that glycosylation at N49, N58, N74, and N116 does not overlap with the bind epitopes of NB01 or 136B4 Abs and would not interfere with Ab interaction with PD-1 (Fig. 2 F).

The epitope mapping and structural studies both revealed that Ab binding to a specific region of PD-1 on the opposing face of the PDL-1–PDL-2 interaction site resulted in an antagonistic functional activity (Fig. 1 and Fig. 2, C and E). Interestingly, sequence alignment across five species revealed that despite a low 52.3% identity with human PD-1, conserved regions throughout the sequence come together to form a highly conserved patch on PD-1 (Fig. S3 B) that is partially overlapping with the binding epitopes of both 135C12 (NB01 hIgG4) and 136B4 Abs (P1 patch in Fig. 2 F).

Structural models of hPD-1–NB01a Fab with either pembrolizumab (PDB accession no. 5GGS) or nivolumab (PDB accession no. 5GGR) were also generated and clearly show that NB01a can bind hPD-1 simultaneously with either PDL-1 blocking Ab (Fig. 2 G; Lee et al., 2016). This model is consistent with our Ab competitive binding studies (Fig. 2 D).

Nonblocking and blocking anti–PD-1 Abs synergize in recovering Ag-specific CD8 T cells from exhaustion

Given that nonblocking anti–PD-1 Abs can bind simultaneously to cell-surface PD-1 with blocking Abs such as pembrolizumab, an important question is whether the simultaneous binding results in a synergistic potentiation of their antagonistic activity. This was addressed by testing combinations of blocking and nonblocking Abs in the in vitro functional recovery exhaustion assay. Studies presented in Fig. 3 show a significant increase in the recovery of proliferation of HIV-specific CD8 T cells when NB01a was used in combination of either pembrolizumab or B01 with 155% and 158% proliferating cells, respectively, relative to single Abs. These increases in proliferation were observed with the 135C12 mouse IgG1 variants of NB01 and several different humanized IgG4 clones (Fig. S2, A–D). It is important to underscore that this enhanced proliferation was beyond levels that could be achieved by higher Ab concentrations or with combinations of two blocking Abs that did not lead to enhancements in the recovery of proliferation (Fig. S2, E and F).

To further determine the biological activity of the two classes of anti–PD-1 Abs, the synergistic effect of the combination of blocking and nonblocking anti–PD-1 Abs was
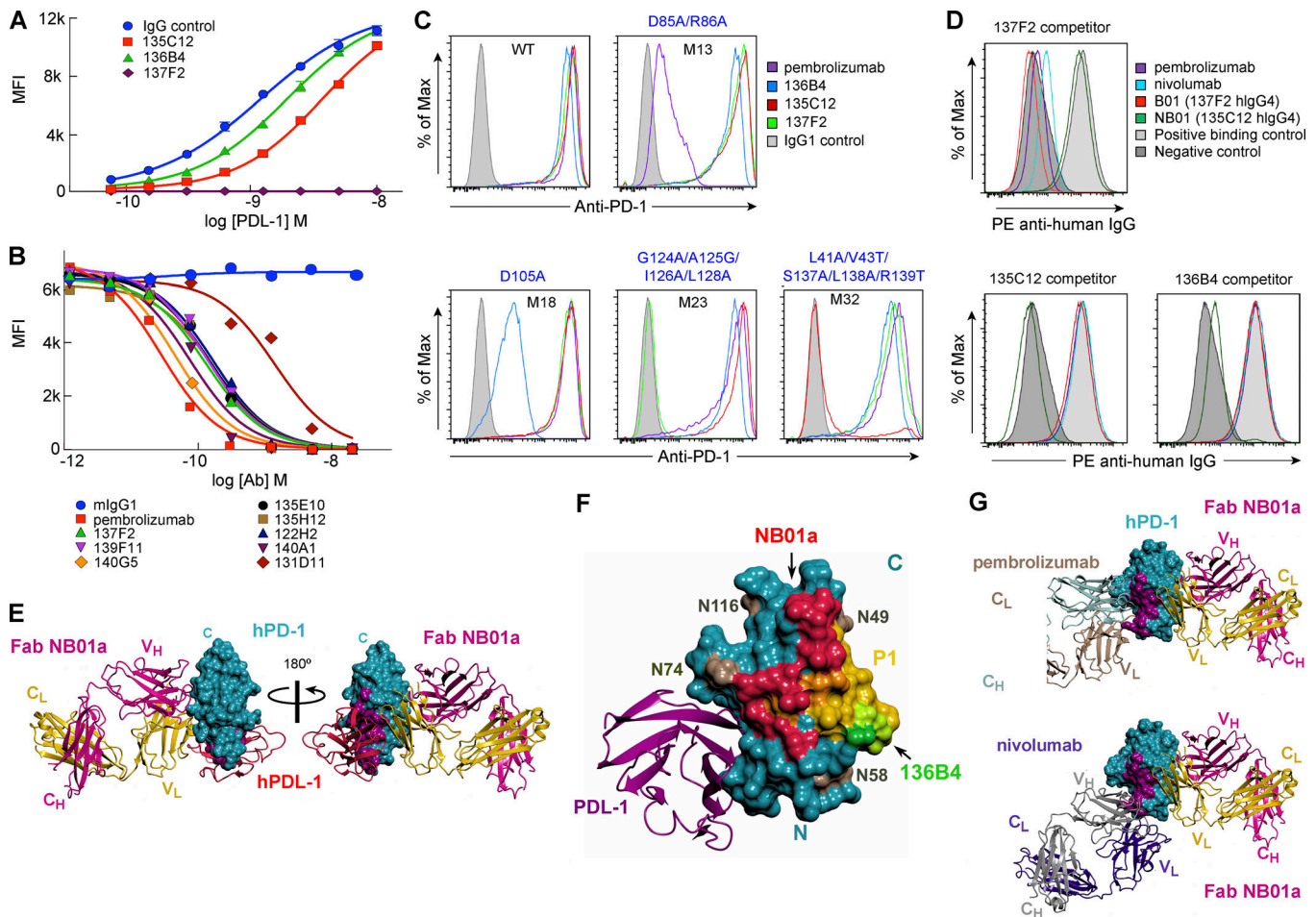
Figure 2. Epitope mapping and structural studies of the prioritized anti–PD-1 Ab clones. (A) Ability of anti–PD-1 Abs to block the PD-1–PDL-1 interaction in a Luminex biochemical assay. PD-1–coated beads were incubated in the presence or absence of a competitor anti–PD-1 Ab, and then beads were stained with different concentrations of biotin-labeled PDL-1 protein. Data (n = 2) are mean ± SD. MFI, mean fluorescence intensity. **(B)** Potency of anti–PD-1 Abs in blocking the PD-1–PDL-1 interaction in a Luminex biochemical assay. PD-1–coated beads were incubated with a fixed concentration of PDL-1 equivalent to the half-maximal inhibitory concentration value for the PD-1–PDL-1 interaction in this assay. The PD-1–PDL-1 complex, bound at 50% in equilibrium, was then treated with increasing concentrations of anti–PD-1 Ab to determine if they were capable of completely disrupting the PD-1–PDL-1 interaction with pembrolizumab used as a positive blocking Ab control. **(C)** Epitope mapping by site directed mutagenesis of PD-1. Defined epitopes were identified for anti–PD-1 Abs that were either blocking or nonblocking of the PD-1–PDL-1 interaction using HeLa cells transfected with expression vectors encoding PD-1 with substitutions at solvent accessible residues. Amino acid substitutions in PD-1 are indicated in blue lettering above each histogram. Representative data are shown for n = 3 experiments. **(D)** Ab competitive binding studies for cell-surface PD-1. Jurkat PD-1 cells were incubated with excess of 137F2, 135C12, or 136B4 mouse Abs and then stained with a minimal concentration of the indicated humanized anti–PD-1 Abs (n = 3). **(E)** hPD-1 and NB01a Fab (humanized version of the mouse 135C12 Ab) complexes were purified by size-exclusion chromatography and crystallized. Crystals diffracted to 2.2 Å resolution, and the structure was solved by molecular replacement. The structure reveals that the binding site of NB01a is adjacent to residues in purple involved in the PD-1 interaction with either PDL-1 or PDL-2. The CC′ loop (residues 70–74) of hPDL-1 is disordered and indicated as a dashed line. Loops connecting β strands BC (57–63), C′D (84–92), and FG (127–133) were also disordered. Strands are named following the canonical designation. Cα superpositioning of the hPD-1 present in the NB01a Fab and hPDL-1 (PDB accession no. 4ZQK) complexes show that NB01a Fab and PDL-1 bind distinct nonoverlapping sites on PD-1. **(F)** Mapping of variable residues between human PD-1 and monkey, dog, horse, mouse, and rat PD-1 revealed an evolutionarily conserved patch (P1) on the opposite face of PD-1 from the PDL-1 or PDL-2 interaction site (yellow, orange, and light green colored residues). The P1 patch overlaps with the binding epitopes for the 135C12/NB01 (orange residues) and 136B4 (light green residues) antagonistic Abs that are nonblocking of PD-1–PDL-1. Residues N49, N58, N74, and N116 that are predicted N-linked glycosylation sites are show in brown on the PD-1 model to be excluded from the P1 patch, 135C12/NB01, and 136B4 Ab binding epitopes. **(G)** Cα superpositioning of hPDL-1 coordinates of the NB01a complex with pembrolizumab (PDB accession no. 5GGS) and the nivolumab (PDB accession no. 5GGR) confirms that NB01a Fab binding to PD-1 does not interfere with the binding of either pembrolizumab or nivolumab anti–PD-1 Abs. hPDL-1 is shown as a ribbon diagram in E and F, with the hPDL-1 binding surface (PDB accession no. 4ZQK) colored in purple in G.

assessed on the production of cytokines. For these purposes, blood mononuclear cells from eight chronically infected viremic HIV individuals were stimulated with the specific antigenic peptides. Cells treated with anti–PD-1 Ab combinations released significantly higher levels of IFNγ, TNFα, and IL-10

relative to antigenic peptide alone treatments (Fig. 3 B). Additionally, results across the different donors showed that Ab combination treatment lead to IFNγ production with significantly higher levels than either blocking or nonblocking anti–PD-1 monotherapy treatments alone.

A

Patient C10

B
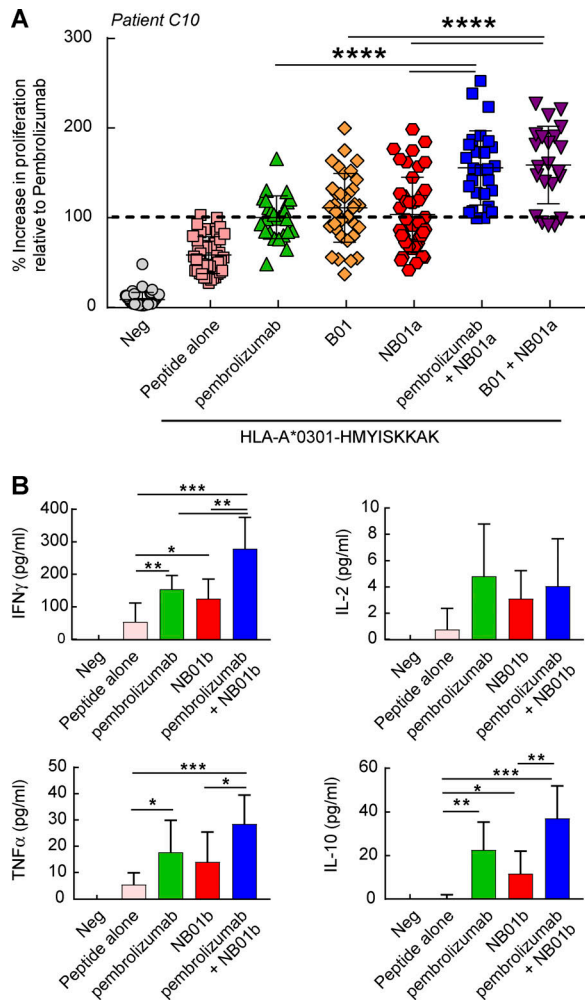
Figure 3. Blocking and nonblocking anti–PD-1 Ab combinations synergize in recovering both the proliferation and functional activity of exhausted Ag-specific CD8 T cells. (A) Cumulative results (three to six experiments) of the recovery of the proliferation of HIV-specific CD8 T cells after treatment with single and/or the combination of blocking and/or nonblocking anti–PD-1 Abs. Results are expressed as the percentage of CFSE-low CD8 T cells, and 8–10 replicates were performed for each experimental condition. **(B)** Recovery of T cell functionality evaluated by measuring cytokine levels of IFNγ, IL-2, TNFα, and IL-10 in the cell medium following an Ag-specific CD8 T cell stimulation. Cumulative results are shown using the PBLs from six to eight different viremic HIV-positive donors. Untreated samples (Neg) were used as a negative control in each experiment. Data represent mean ± SD. *, $P < 0.036$; **, $P < 0.0079$; ***, $P < 0.0009$; ****, $P < 0.0001$ (unpaired t test with Welch's correction).

Nonblocking anti–PD-1 Abs act predominantly through the CD28 costimulatory receptor to promote the AKT–NF-κB pathway

Mechanism-of-action studies with anti–PD-1 Abs were then investigated using phosphoflow intracellular staining of proteins important to the T cell signaling cascade. Blood mononuclear cells from a viremic HIV-positive donor were used for these signaling studies with 60–63% of memory T cells expressing the PD-1 exhaustion marker. T cell stimulation with anti-CD3/CD28 Abs induced a temporal increase in protein phosphorylation that was proximal to (ZAP70, SLP76, and Lck/Src) and downstream

of (AKT, PDK1, PLCγ1, NF-κB, ERK1/2, p38, and CREB) the TCR complex. T cell signaling was suppressed with human PDL-1 Fc fusion protein when added before the anti-CD3/CD28 stimulation. Importantly, this protocol using exhausted primary T cells identified the same canonical pathways reported for PDL-1–PD-1 mediated suppression of T cell activation using immunoblotting techniques that were performed with cell lines or in vitro stimulated T cell to augment PD-1 expression (Patsoukis et al., 2012; Yokosuka et al., 2012). T cell stimulation in the presence of PDL-1 resulted in statistically significant reduced phosphorylation of ZAP70 and Lck394/Src 1 min after stimulation and ERK1/2, AKT, and PDK1 5–15 min after stimulation (Figs. 4 A and S4).

Pretreatment of cells with NB01b or pembrolizumab partially restored phosphorylation of PDK1-pS242, AKT-pT308, and AKT-pS473 when stimulated with anti-CD3/CD28 in the presence of PDL-1 Fc protein. A trend toward recovery was also observed with ERK1/2, ZAP70, and LCK394/Src phosphorylation levels; however, these levels did not reach statistical significance. Anti–PD-1 Ab–mediated rescue was not evident for AKT at the earliest time point evaluated, but phosphorylation levels gradually built to a significant increase at 5 and 15 min for both PDK1 and AKT (Fig. 4 A). This increased phosphorylation was more statistically significant for the nonblocking anti–PD-1 Ab compared with pembrolizumab-treated cells, which also had a trend toward lower phospho-AKT levels 15 min after stimulation. This pathway is directly downstream of the CD28 costimulatory receptor, which was previous reported to be necessary for the antitumor activity of blocking anti–PD-1 Abs (Hui et al., 2017). These results are consistent with a mechanism whereby anti–PD-1 Ab therapy prevents the PDL-1–mediated recruitment of a phosphatase to the PDK1–AKT complex. Prolonged phosphorylation and activation of the PDK1–AKT complex would lead to increased T cell survival, trafficking and effector function.

An important aspect of T cell stimulation is the rapid increase in cytoplasmic levels of calcium (Ca^{2+}) released from intracellular stores and through the opening of the plasma membrane calcium release–activated channels. This Ca^{2+} release helps to propagate the T cell activation signal, including NFAT activation and cytoskeletal rearrangement. Similar to the phospho-flow experiments, stimulation of exhausted PD-1^{+} T cells in the presence of a PDL-1 Fc fusion protein led to reduced levels of intracellular Ca^{2+} relative to an anti-CD3/CD28 Ab stimulation control (Fig. 4, B and C). Pretreatment of cells with either blocking (pembrolizumab or nivolumab) or nonblocking NB01b anti–PD-1 Abs restored Ca^{2+} mobilization to levels observed in cells stimulated in the absence of PDL-1 Fc protein. Importantly, combinations of NB01b and either pembrolizumab (Fig. 4 B) or nivolumab (Fig. 4 C) before T cell stimulation in the presence of PDL-1 resulted in a synergistic increase in Ca^{2+} levels. This Ca^{2+} mobilization was more intense and gave area under the curve values more than twofold higher compared with the anti-CD3/CD28 stimulation condition.

To provide insights on the mechanistic differences in the effect of blocking and nonblocking anti–PD-1 Abs, the two classes of Abs were further probed by immunoprecipitation (IP) of PD-1 expressed on a Jurkat cell line stably expressing high levels of PD-1. Cells were unstimulated or stimulated with anti-

Figure 4. Nonblocking anti–PD-1 Abs restore Ca²⁺ flux and AKT signaling to exhausted T cells. (A) Phospho-flow signaling studies performed with PD-1–expressing functionally exhausted T cells. Intracellular staining of phosphoproteins important to T cell signaling showed increased phosphorylation upon stimulation with anti-CD3/CD28 Abs. FACS histogram profiles for memory CD4 T cells show that a PDL-1 Fc fusion protein suppressed phosphorylation of AKT pT308, AKT pS473, and PDK1 pS242. Preincubation of cells with NB01b nonblocking or pembrolizumab blocking anti–PD-1 Abs significantly relieved PDL-1–mediated suppression of these phosphosignaling proteins at 5 and 15 min after stimulation. Data are presented as mean ± SEM for five to eight individual experiments. ns, not significant; *, P < 0.05; **, P < 0.0064; ****, P < 0.0001. **(B)** Exhausted T cells had reduced Ca²⁺ mobilization when stimulated with anti-CD3/CD28 in the presence of PDL-1 Fc fusion protein. **(C)** This suppression was restored with NB01b, pembrolizumab, or nivolumab. Synergistic increase in Ca²⁺ release was observed in exhausted T cells stimulated with anti-CD3/CD28 + PDL-1 when coincubated with NB01b and either pembrolizumab (B) or nivolumab (C). Representative data are shown from three independent experiments, and clinical Ab preparation of pembrolizumab was used for these studies. FDR, false discovery rate; MFI, mean fluorescence intensity.

CD3/CD28 Abs and then the PD-1 receptor and associated cellular complex was coprecipitated with NB01b, pembrolizumab or a combination of NB01b and pembrolizumab Abs covalently coupled to beads. In stimulated cells, pembrolizumab effectively pulled down a PD-1 complex that included CD28, SHP-2, PI3K, and phosphorylated Src (Fig. 5 A). In contrast, although NB01b pulled down equivalent levels of PD-1 and the PD-1–associated SHP-2 compared with pembrolizumab, there were significantly lower levels of CD28 receptor and PI3K in the nonblocking anti–PD-1 Ab IP complex (Fig. 5, A and B). AKT was weakly immunoprecipitated with the PD-1 complex, but there was a trend toward higher levels of AKT pulled down with pembrolizumab compared with the NB01b Ab. IPs performed with pembrolizumab- and NB01b-coated beads resulted in reduced levels of CD28 being coprecipitated with PD-1 relative to the pembrolizumab-alone IP (Fig. 5 B). In the above experiments, recruitment of PD-1 in the immunological synapse after anti-CD3/CD28 stimulation occurred in the absence of PDL-1 engagement. To explain how the recruitment of PD-1 occurs in the absence of PDL-1 engagement, in control experiments, IPs were performed using biotinylated pembrolizumab and NB01b not coupled to beads. These experiments showed that uncoupled Abs did not pull down the CD28 in either the presence or absence of stimulation (Fig. 5 C). Therefore, these control experiments indicate that aggregation induced by the anti–PD-1 Abs coupled to beads deliver to PD-1 a signal similar to the engagement of PDL-1 and promote recruitment of PD-1 to the CD28 costimulatory receptor following T cell activation as shown in Fig. 5 B.

Taken together, these results indicate that PD-1 is recruited to the CD28 costimulatory receptor upon T cell activation and that this complex is unaffected by the blocking with pembrolizumab anti–PD-1 Ab. Importantly, nonblocking Abs such as NB01b inhibit the formation of the PD-1 complex that includes CD28. This would effectively reduce the recruitment of the SHP-2 phosphatase to the CD28 costimulatory receptor and its associated intracellular kinases that includes PI3K, the upstream activator of AKT (Parry et al., 2005; Patsoukis et al., 2012).

Given that the CD28 costimulatory receptor contributes to T cell activation through enhanced signaling of the AKT–NF-κB pathways and TCR stimulation acts strongly through the NFAT pathway, anti–PD-1 Abs were tested in NF-κB and NFAT reporter assays. A Jurkat–PD-1 T cell line stably expressing luciferase under the control of a NFAT promoter was transiently transfected with the NanoLuc NF-κB reporter plasmid in order to monitor the activation of both pathways in the same cells. Experiments using this cell line were designed to evaluate the potency of blocking anti–PD-1 Abs, and stimulation was achieved through coculture of Jurkat PD-1 cells with 293T cells coexpressing a membrane-associated anti-CD3 TCR activator and the PDL-1 receptor. Pretreating Jurkat PD-1 cells with the blocking pembrolizumab anti–PD-1 Ab before stimulation effectively relieved the PD-1–PDL-1–mediated suppression of the NFAT reporter by 6.4-fold in this assay relative to an IgG4 control Ab, while the NB01b nonblocking anti–PD-1 Ab resulted in low to no NFAT activation (Fig. 5 D). In contrast, parallel evaluation of the NF-κB pathway showed that both blocking and nonblocking

anti–PD-1 Abs significantly relived PD-1–mediated suppression of the NF-κB promoter following TCR-mediated activation (1.7-fold and 2.4-fold relative to an IgG4 isotype control, respectively; Fig. 5 D). Consistent with the functional data (Fig. 3, A and B) and Ca²⁺ flux studies (Fig. 4, B and C), combination of blocking and nonblocking anti–PD-1 Abs result in a significant increase in NFAT activation relative to single anti–PD-1 Ab treatments given alone.

Taken together, signaling and IP studies show that classical blocking and antagonistic nonblocking anti–PD-1 Abs act through distinct mechanisms in relieving T cell exhaustion. Both Ab classes are shown to act on pathways linked to PD-1–mediated suppression of T cell activation. However, blocking Abs have a more pronounced effect on the NFAT pathway, while nonblocking Abs act predominantly through the CD28 coreceptor that promotes the AKT–NF-κB pathway and leads to T cell proliferation and survival.

In vivo efficacy of nonblocking anti–PD-1 Abs

The antagonistic activity of PDL-1 nonblocking Abs and the synergistic effect observed in vitro provided the scientific rationale to determine the ability of nonblocking Abs alone or in combination with blocking Abs in suppressing tumor growth in vivo. The in vivo efficacy of the NB01b antagonistic nonblocking Ab was then evaluated in the PD-1 HuGEMM in vivo tumor model (Lute et al., 2005; Huang et al., 2017). HuGEMM mice were genetically engineered to express a chimeric human/mouse PD-1 protein with the majority of the ectodomain (residues 26–146) encoded by the human PD-1 protein. Mice successfully engrafted with tumors formed from the PDL-1–high MC38 colon adenocarcinoma cell line were randomly ascribed to give the same average tumor volumes for the different arms of the study with the indicated treatments administered twice weekly (Fig. 6 A). The nonblocking NB01b Ab administered at 10 mg/kg effectively suppressed tumor growth similar to pembrolizumab (clinical Ab batch) or nivolumab administered at the same dose in three separate studies (Fig. 6, B–D and F). We then determined whether the antitumor activity was enhanced by combining NB01b and either pembrolizumab or nivolumab. Mice that were coadministered with NB01b and pembrolizumab or nivolumab at a dose of 5 mg/kg of each Ab, for a total dose of 10 mg/kg, had more potent suppression in tumor growth relative to either Ab dosed alone (Fig. 6, E and F). A global analysis of three separate studies was performed where mice were treated with NB01b, pembrolizumab, and nivolumab monotherapies or combination therapies consisting of NB01b with either pembrolizumab or nivolumab. This analysis showed that the combination of blocking and nonblocking anti–PD-1 Abs was associated with a significantly greater suppression of tumor growth throughout the study. In modeling the cubic root–transformed tumor volumes as a function of time and Ab therapy using a mixed-effects statistical framework (Fig. 6 F), it can be seen that Ab combination therapy had a significant reduction in tumor volume over time compared with the anti–PD-1 monotherapy arms in the studies (P = 0.00045). Importantly, the proportion of mice with complete control of tumor growth, having a smaller tumor volume at the end of the study compared

Fenwick et al.
Enhanced anti–PD-1–mediated immune recovery

Journal of Experimental Medicine
https://doi.org/10.1084/jem.20182359

1531
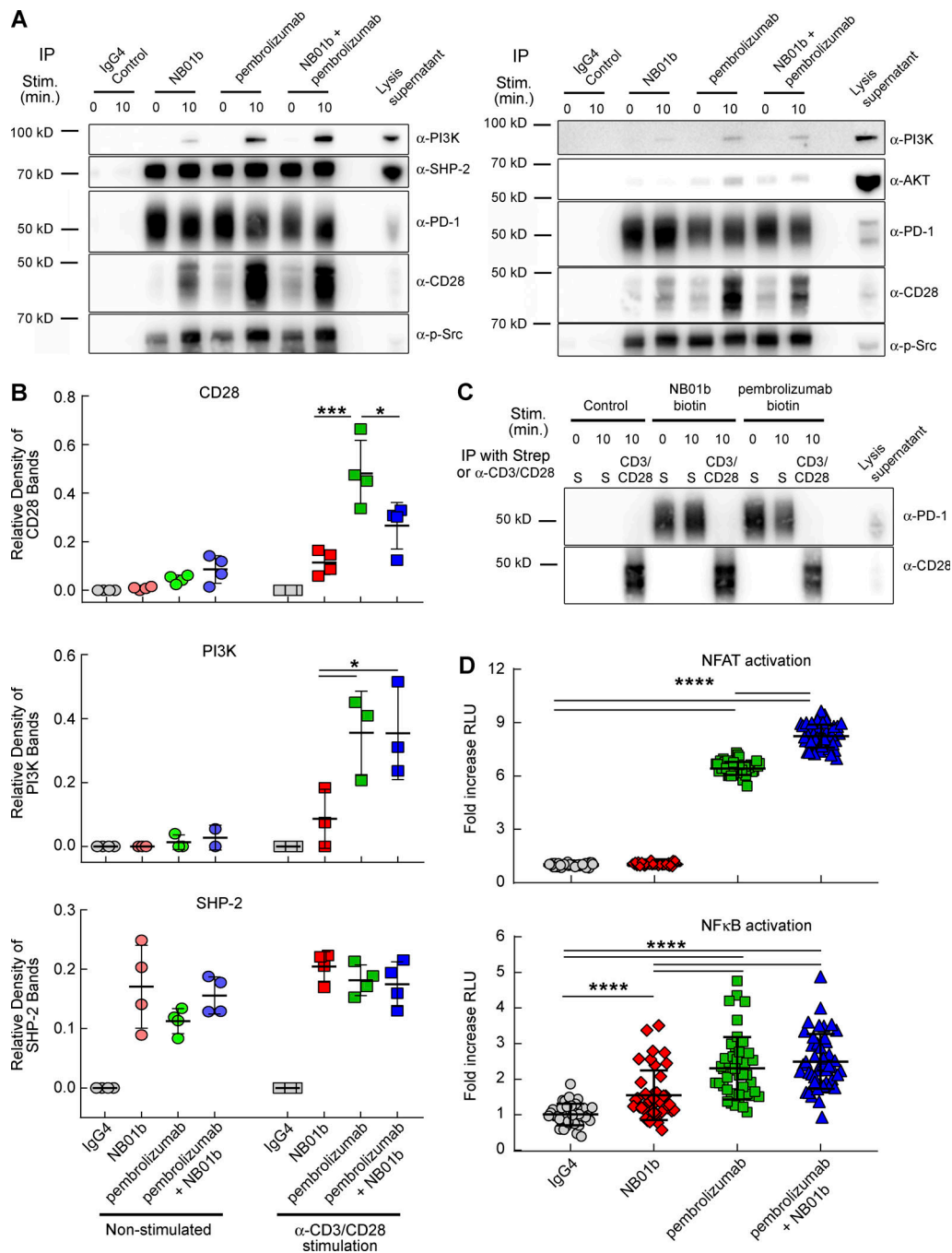
Figure 5. **Nonblocking anti–PD-1 Abs act primarily through the CD28 costimulatory receptor–associated pathway. (A)** IPs for two representative experiments are shown where the PD-1 receptor and associated protein complex were immunoprecipitated with NB01b, pembrolizumab, or a combination of NB01b and pembrolizumab in nonstimulated and anti-CD3/CD28 Ab–stimulated Jurkat PD-1 cells. In stimulated cells, pembrolizumab coprecipitated high levels of PD-1, CD28, SHP-2, PI3K, and the phosphorylated form of Src (p-Src) with the PD-1 complex. **(B)** NB01b pulled down equivalent levels of PD-1, SHP-2, and p-Src, but significantly reduced levels of CD28 and PI3K were observed in three or four separate experiments. AKT was only weakly pulled down in the PD-1 complex (A; right blot); however, there was a trend toward higher levels of AKT being immunoprecipitated with pembrolizumab compared with NB01b. **(C)** Control IPs performed by preincubating cells with either biotinylated pembrolizumab or NB01b before T cell stimulation shows that PD-1 pulled down with streptavidin (S) does not constitutively form a complex with CD28. Similarly, IPs performed with anti-CD3/CD28 coated beads show a strong pull-down of CD28 without detectable levels of associated PD-1. **(D)** The nonblocking anti–PD-1 Ab NB01b showed weak to no activation of the NFAT promoter in a Jurkat PD-1 luciferase reporter cell line when stimulated with 293T cells coexpressing a TCR activator and the PDL-1 receptor. Pretreatment of Jurkat PD-1 cells with the blocking anti–PD-1 Ab pembrolizumab strongly promoted NFAT activation. In contrast, both NB01b and pembrolizumab relieved PD-1–mediated suppression of NF-κB activation. Graphs show the mean ± SD and are representative of two independent experiments. *, P < 0.045; ***, P < 0.001; ****, P < 0.0001 (unpaired t test with Welch's correction). RLU, relative luminescence units.
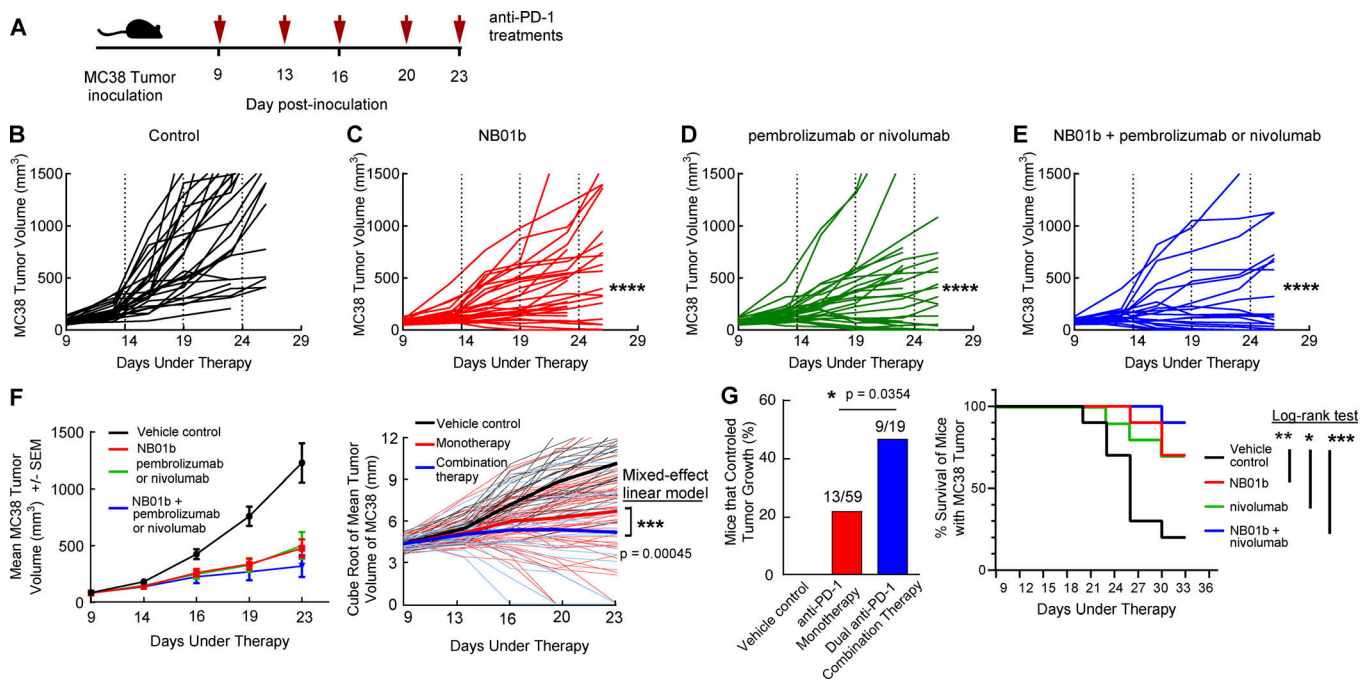
Figure 6. Enhancement of tumor clearance by the combination of blocking and nonblocking anti–PD-1 Abs in the PD-1 HuGEMM in vivo MC38 tumor model. (A) Experimental scheme. **(B–E)** Mice successfully engrafted with the MC38 tumor cell line were treated twice weekly with PBS control (B), NB01b (C), pembrolizumab or nivolumab (D), or a combination of NB01b with either pembrolizumab or nivolumab (E), with tumor volumes measured in parallel. A collective analysis of three separate studies with n = 9–10 mice per arm per study is presented in A–D. P values determined by pairwise comparison using a mixed-effect linear model showed that all Ab arms of the study had reduced tumor growth compared with the vehicle control arm. **(F)** Suppression of tumor volume in mice engrafted with PDL-1–high MC38 cell line with either single or the combination of blocking and nonblocking anti–PD-1 Abs. Blocking (pembrolizumab or nivolumab) and nonblocking (NB01b) anti–PD-1 Ab monotherapies exerted equivalent suppression of tumor growth and mean percent tumor inhibition. Modeling of the cubic root transformed tumor volume in three separate studies as a function of time demonstrated a statistically significant reduction in tumor volume over time for the anti–PD-1 combination therapy relative to anti–PD-1 monotherapies. **(G)** Combination anti–PD-1 Ab therapy significantly enhanced the proportion of mice that controlled tumor growth (9 out of 19 mice) relative to Ab monotherapies (13 out of 59 mice). Survival analysis for a study performed using NB01b and nivolumab, with statistical differences determined using the log-rank test. Graphs show the mean ± SEM, unless otherwise indicated. *, P = 0.0223; **, P < 0.008; ***, P = 0.0005; ****, P < 0.0001.

with the initial day of anti–PD-1 therapy, was 47% (9 out of 19 mice) in the combination treatment group (NB01b plus pembrolizumab or nivolumab) Abs as compared with 22% (13 out of 59) in the anti–PD-1 Ab monotherapy treatment groups (Fig. 6 G; P = 0.0354). In a study that was extended to 33 d after MC38 inoculation, mouse survival was significantly improved for the combination therapy arm relative to vehicle control–treated mice (Fig. 6 G; P = 0.0005). The significance of this extended survival was greater for the combination therapy relative to either NB01b or nivolumab monotherapies administered alone (Fig. 6 G, 0.0079 and 0.0223, respectively).

In a second in vivo study, PD-1 HuGEMM mice were subcutaneously implanted with the highly aggressive and poorly immunogenic wild-type B16F10 cell line (Kuzu et al., 2015; Kokolus et al., 2017). B16F10 tumor, which is engrafted subcutaneously, is characterized by a very fast growth and generation of rapid lung metastasis. As for the MC38 tumor model, mice were dosed twice weekly with blocking pembrolizumab, nonblocking NB01b, and/or the combination of both blocker/nonblocker Abs (Fig. 7 A). Suppression of tumor growth in the active groups versus the vehicle control untreated group was similar (Fig. 7, B–E). Although the suppression of tumor growth was significant (P < 0.008) in the active groups, the effect was transient and

associated with rapid escape of the tumor. Furthermore, significant prolonged mouse survival was observed in the active groups as compared with the vehicle control group as determined using a log-rank statistical test (Fig. 7 F).

Discussion

Here, we report the identification of a novel class of antagonistic anti–PD-1 Abs acting independently of PDL-1 blockade. These Abs were rare among hybridoma clone–producing Abs with high affinity for PD-1 (3.2% of 156 clones), which may partially explain why this novel anti–PD-1 Ab class has eluded discovery until now. Given the prevailing theory that PD-1–PDL-1 blockade is an important element needed for relieving T cell exhaustion, we performed several different lines of investigation to validate that our novel anti–PD-1 Abs were truly nonblocking of the PD-1–PDL-1 interaction.

Protein-to-protein (PD-1–PDL-1) interaction studies, together with competitive binding studies using the Jurkat PD-1 stable cell line, provided evidence that 135C12 or 136B4 nonblocking Abs interfere neither with the PD-1–PDL-1 interaction nor with the simultaneous binding of blocking Abs to PD-1 expressed at the cell surface. These results indicate that

Fenwick et al.
Enhanced anti–PD-1–mediated immune recovery

Journal of Experimental Medicine
https://doi.org/10.1084/jem.20182359

1533
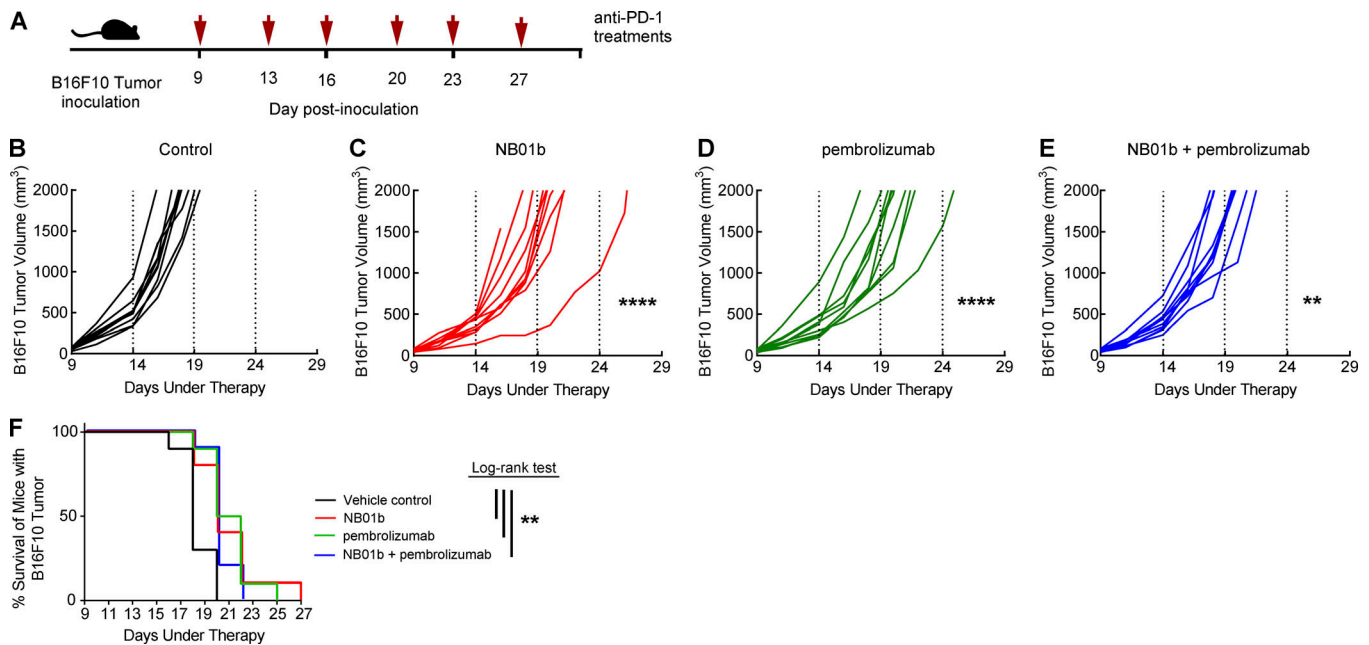
Figure 7. **Blocking and nonblocking anti–PD-1 Abs suppress tumor growth and prolong survival of mice implanted with B16F10 cells in the PD-1 HuGEMM in vivo tumor model. (A)** Experimental scheme. **(B–E)** Mice successfully engrafted with the poorly immunogenic B16F10 tumor cell line were treated twice weekly with PBS control (B), NB01b (C), pembrolizumab (D), or a combination of NB01b and pembrolizumab (E), with tumor volumes measured in parallel in the treatment (n = 10 mice) and control (vehicle; n = 10 mice) groups. P values determined by pairwise comparison using a mixed-effect linear model showed that blocking (pembrolizumab), nonblocking (NB01b), and combination anti–PD-1 Ab therapies had reduced tumor volume growth relative to the vehicle control. **(F)** Survival analysis with statistical difference determined using the log-rank test. Graphs show the mean ± SEM. **, P = 0.008; ****, P < 0.0001.

nonblocking anti–PD-1 Abs do not sterically interfere with PDL-1 binding to PD-1 and do not exert a conformational change to the PD-1 protein that would significantly reduce its affinity for the PDL-1 ligand, and they exclude the possibility that either conformational or posttranslational differences occur between recombinant PD-1 and the cell-surface PD-1 receptor.

Epitope mapping studies performed through PD-1 site-directed mutagenesis together with the hPD-1–NB01a Fab crystal structure have shown that the novel two nonblocking anti–PD-1 Abs with antagonistic activity both bind PD-1 on different epitopes located on the opposing face of PD-1 relative to the PDL-1 interaction site. Importantly, we discovered that this novel functional active region of PD-1 recognized by nonblocking Abs overlaps with a patch of PD-1 residues that are highly conserved across six different species. Evolutionary conservation of this region suggests that PD-1 is under a selective pressure to preserve this site, which could be explained by the site being functionally implicated in PD-1 signaling or potentially through interaction with an alternate ligand from PDL-1–PDL-2. The fact that 135C12/NB01 and 136B4 Abs both overlap with an edge of this conserved site on PD-1 indicates that steric blocking of an alternate ligand and/or a complex formed with CD28 may represent the most likely hypothesis.

Consistent with blocking and nonblocking Abs both exerting distinct immune-enhancing functional activity through PD-1, combination therapy using the two classes of anti–PD-1 resulted in synergistic functional recovery of Ag-specific CD8 T cells from exhaustion.

Mechanism-of-action studies demonstrated that blocking and nonblocking anti–PD-1 Abs relieve PD-1 mediated T cell exhaustion through distinct effects on the TCR and CD28 related signaling cascades. We have provided evidence that the blocking Abs have a more pronounced effect on the NFAT pathway, while nonblocking Abs act predominantly through the CD28 coreceptor that promotes the AKT–NF-κB pathway. Previous studies (Patsoukis et al., 2012, 2013; Yokosuka et al., 2012; Hui et al., 2017) have indicated that PD-1 exerts its suppressive effects on T cell activation through PDL-1–mediated recruitment of PD-1 into the immunological synapse. This recruitment brings the PD-1–associated SHP-2 phosphatase into contact with the TCR-associated kinases, including ZAP70, Lck/Src, and ERK1/2, thus resulting in dephosphorylation of these kinases and dampening the intensity and duration of the T cell–specific activation. Blocking anti–PD-1 and anti–PDL-1 Abs relieve T cell exhaustion by preventing this recruitment of PD-1 into the TCR complex (Chemnitz et al., 2004; Sheppard et al., 2004; Yokosuka et al., 2012; Wherry and Kurachi, 2015; Hui et al., 2017; Kamphorst et al., 2017). Interestingly, our IP studies performed with the blocking anti–PD-1 Ab pembrolizumab showed that a complex formed between PD-1 and CD28 upon T cell activation. This indicates that elevated levels of PD-1 on a T cell may suppress TCR activation by a second mechanism, whereby PD-1 forms a cis complex with the CD28 costimulatory receptor. This colocalization would bring CD28-associated intracellular kinases essential for T cell costimulation into contact with

PD-1–associated SHP-2 phosphatase, resulting in a reduced costimulatory effect. In contrast, IPs performed with the non-blocking anti–PD-1 NB01b show significantly lower levels of a PD-1–CD28 complex after T cell activation. Taken together, our results support the model that in binding PD-1 on the opposing face of the PDL-1 interaction site, NB01b disrupts the inhibitory close-contact complex that forms between PD-1 and CD28 on activated T cells. The importance of this PD-1–CD28 interaction may explain the evolutionary conservation of the residues on PD-1 overlapping with the binding site of the nonblocking Abs. Our results are also consistent with Hui et al., who recently demonstrated that CD28 is the primary substrate for dephos-phorylation through PD-1/SHP-2, leading to T cell suppression (Hui et al., 2017).

The distinct mechanism of nonblocking anti–PD-1 Abs may also help rationalize our in vitro functional data, where there is a trend toward lower cytokine production with NB01b compared with pembrolizumab. Since nonblocking Abs have a more limited effect on restoring PD-1–mediated suppression of the NFAT–Ca^{2+} flux pathways, one would predict a reduced enhancement in cytokine production. Conversely, the more pronounced effect of nonblocking anti–PD-1 Abs on the AKT–NF-κB pathway is consistent with the enhanced proliferation observed when used in combination with blocking anti–PD-1 Abs.

The finding that blocker and nonblocker Abs act through distinct mechanisms explains the synergistic effect observed both in vitro and in vivo studies in combining the two classes of Abs. We have provided three lines of evidence in in vitro studies on the synergistic effect using a combination of blocking and nonblocking anti–PD-1 Abs: (1) increased Ag-specific CD8 T cell proliferation, (2) increased cytokine production in response to Ag-specific stimulation, and (3) enhanced intracellular Ca^{2+} mobilization following anti-CD3/CD28 stimulation in the presence of PDL-1 suppression.

The immunotherapy with anti–PD-1 Abs is a major breakthrough in the fight against cancer, and anti–PD-1 therapy using pembrolizumab or nivolumab achieves a 20–50% objective response rate depending upon the type of cancer and the selection of criteria used for determining the percentage of PDL-1–expressing tumor cells (Carbognin et al., 2015; Gandini et al., 2016). Many patients have only a partial response to treatment, and a variable proportion of patients (depending on the type of cancer) experience recurrence of the tumor. Therefore, it has become clear that the potentiation of the antitumor activity of blocker anti–PD-1 Abs and the development of combinations of immunotherapy strategies are urgently needed. In addition to combination of anti–PD-1 Abs with anti–CTLA-4 (Larkin et al., 2015), combination therapies with Abs targeting other immune checkpoint inhibitors have entered clinical development.

In the present study, we have shown in two in vivo mouse tumor models that the novel nonblocking anti–PD-1 Abs have an antitumor activity equal to the conventional blocking Abs such as pembrolizumab. We have validated the results using the immunogenic colon carcinoma MC38 cell line and the highly aggressive and poorly immunogenic melanoma B16F10 cell line. Of note, in the MC38 studies, combination therapy using both classes of anti–PD-1 Abs significantly suppressed tumor growth

(74%) and was associated with a 2.4-fold increase in mice with complete tumor control and a trend toward improved survival relative to anti–PD-1 monotherapies.

The antitumor activity in the B16F10 model observed with anti–PD-1 monotherapy using either blocking or nonblocking Abs was inferior and transient as compared with MC38 model. The limited antitumor effect observed in our study is consistent with previous studies (Chen et al., 2015; Woods et al., 2015; Zamarin et al., 2018) in the B16F10 tumor model using anti–PD-1 treatment. Along the same line, combination of blocking and nonblocking Abs did not provide an additional therapeutic advantage in the poorly immunogenic B16F10 model. This may be attributed to the exceptionally rapid growth of the B16F10 cells, where tumor volume was >1,000 mm³ in 70% of mice in the vehicle control arm by day 7 after initiation of anti–PD-1 therapy. Because of the rapid tumor escape, there is likely not sufficient time to develop a fully competent immune response and allow for the combined anti–PD-1 treatment to enhance tumor suppression, since only two doses of the combined treatment were administered by day 7. It should be underscored that this high rate of tumor growth in the B16F10 mouse tumor model is not representative of tumor development in humans.

In conclusion, we report the identification of a novel class of antagonistic anti–PD-1 Abs acting independently of PDL-1 blockade and acting through the CD28–AKT–NF-κB costimulatory pathway. These nonblocking anti–PD-1 Abs synergize with the classical blocker anti–PD-1 and are associated with an improvement of antitumor activity. These results provide important advances in the biology and function of PD-1 and may open new avenues for enhanced antitumor activity.

Materials and methods

Abs
Novel mouse anti–PD-1 Abs were isolated from the media of hybridoma cell lines and tested for binding to human PD-1 protein in the Luminex assay described below. For hybridomas that produced Abs with affinity < 1 nM, RNA was extracted using the Rneasy micro kit (Qiagen) followed by cDNA synthesis with the Cellsdirect 1-step QRT-PCR kit (Thermo Fisher Scientific) using the mouse Ig-Primer set (EMD Biosciences). The heavy-chain CDR region for each hybridoma was PCR amplified using the mouse Ig-Primer sets and then sequenced using the Applied Biosystems 3500 Genetic Analyzer sequencer (Thermo Fisher Scientific) with sequences described in a patent application (Pantaleo and Fenwick, 2016). Prioritized clones were expressed from 200 ml of hybridoma cells with the monoclonal Abs purified from the cell medium using a protein A column (Thermo Fisher Scientific) with Abs eluted with a 100 mM glycine buffer pH 3.0 into a 1 M Tris-HCl eluate at pH8.0. Abs were dialyzed twice against PBS, concentrated using a JumboSep centrifuge filter with a 3-kD molecular weight cutoff (Pall Laboratories) and sterile filtered with a Millex GP 0.22 μm filter (Millipore). Prior to anti–PD-1 Ab evaluation in the in vitro functional recovery assay, Abs were tested with the Food and Drug Administration–licensed Endosafe-PTS kit (Charles River Laboratory), and all had low endotoxin levels at <5 EU per mg of protein.

Fenwick et al.
Enhanced anti–PD-1–mediated immune recovery

Journal of Experimental Medicine
https://doi.org/10.1084/jem.20182359

1535

Humanized Abs of the 135C12 and 137F2 mouse clones were produced by GenScript with the Deluxe Antibody Humanization Service and using a framework assembly method. Briefly, frameworks of different human germlines with high sequence identities for each of the mouse anti–PD-1 Abs were selected and assembled using overlapping PCR. The resulting libraries of humanized Fabs with different framework sequences and encoding the mouse Ab CDR sequences for either 135C12 or 137F2 were then used to generate a phage display library encoding panels of humanized Fabs. Panning the library against the human PD-1 Fc fusion protein (R&D Systems) allowed for the enrichment of binding constructs and individual clones were screened for affinity using a phage ELISA assay. The FASEBA screen (fast screening for expression, biophysical properties, and affinity) was employed to identify Fab fragments that expressed well and had good biophysical properties, with candidate clones ranked based on their dissociation rate after binding to the PD-1 Fc fusion protein in a Biacore T200 assay (GE Healthcare). Candidate sequences with low-binding off rates were transferred into a proprietary vector at GenScript to produce the humanized anti–PD-1 Abs with an IgG4 Fc region that encoded a serine 228 to proline substitution in the hinge region to help prevent in vivo Fab arm exchange. High-affinity humanized clones NB01a, NB01b, and NB01c were identified for the 135C12 Ab and B01 for the 137F2 Ab. Pembrolizumab and nivolumab used in the in vitro functional studies were produced by GenScript using codon-optimized genes to express IgG4 Abs. A clinical lot of pembrolizumab was used in the in vivo mouse studies and was obtained through the Hospitalier Universitaire Vaudois.

The following Abs were used in flow cytometry and Luminex binding studies: allophycocyanin (APC)–H7–conjugated anti-CD3 (clone SK7), Pacific blue–, FITC-, or PE-CF594–conjugated anti-CD4 (clone RPA-T4), anti-CD8 Pacific blue (clone RPA-T8) Abs (Becton Dickinson); PE-labeled goat anti-mouse IgG secondary, PE-labeled F(ab′)2-goat anti-mouse IgG secondary Ab, and mouse IgG1 isotype control (P3.6.2.8.1; eBioscience); PE-labeled goat anti-human IgG secondary Ab (Invitrogen); human IgG4 Isotype control Ab (ET904; Eureka Therapeutics); anti–PD-1 Ab (clone EH12.2H7) and PE-labeled streptavidin (BioLegend) and energy-coupled dye (phycoerythrin–Texas red conjugate)–conjugated anti-CD45RA (clone 2H4; Beckman Coulter).

Phospho-flow and Ca^{2+} signaling studies were performed with the following Abs: CD3 Alexa Fluor 700 (UCHT1; BD), CD4 Qdot 605 (S3.5; Thermo Fisher Scientific), CD8 APC-eFluor780 (RPA-T8; eBioscience), CD8 PerCP-Cy5.5 (SK1; BD), and CD45RA Brilliant violet 650 (HI100; BioLegend) was used for surface T cell characterization. For PD-1 staining of humanized mAbs, goat anti-human PE secondary (Thermo Fisher Scientific) was used. For intracellular phosphoprotein staining, ZAP70 pY319 PE-Cy7 (17A/P-ZAP70; BD), Erk1/2 pT202/pY204 PE-CF594 (20A; BD), SLP76 pY128 Alexa Fluor 488 (J141-668.36.58; BD), p38 pT180/pY182 PE-CF594 (36/p38; BD), PLCγ1 pY783 (27/PLC; BD), AKT pS473 Brilliant violet 421(M89-61; BD), AKT pT308 PE (J1-223.371, BD), PDK1 pS241 Alexa Fluor 647 (J66-653.44.17; BD), NF-κB p65 pS529 Alexa Fluor 488 (K10-895.12.50;

BD), CREB pS133 PE (J151-21; BD), Src pY418 Alexa Fluor 488 (K98-37; BD), Lck505 pY505 Alexa Fluor 647 (4/LCK-Y505; BD), and S6 pS235/236 PE-Cy7 (D57.2.2E; Cell Signaling Technology) were used. For stimulation conditions, anti-CD3 (OKT3; BD), anti-CD28 (CD28.2; BD), and goat anti-mouse secondary Ab (Jackson ImmunoResearch) was used. Recombinant Fc chimeric PDL-1 protein (R&D Systems) was resuspended in PBS and used for suppression experiments. Fluo-4 AM (Thermo Fisher Scientific) was used for calcium flux experiments.

Immunoblot studies were performed with the Abs against PD-1 (D4W23), CD28 (D2Z4E), PI3K (19H8), and pSRC (D49G4) from Cell Signaling Technology and against SHP-2 (79) and AKT (M89-61) from BD Biosciences. Detection of primary Abs used the anti-mouse IgG or the anti-rabbit IgG HRP-linked Abs (catalog numbers 58802 and 7074, respectively; Cell Signaling Technology).

Cell culture
Peripheral blood mononuclear cells were cultured in Roswell Park Memorial Institute (RPMI) medium and HeLa cells in DMEM (GIBCO BRL Life Technologies), each containing 10% heat-inactivated FBS or 6% human serum as indicated (both from Institut de Biotechnologies Jacques Boy), 100 IU/ml penicillin, and 100 µg/ml streptomycin (Bio Concept). Incubation of cells was performed at 37°C with 5% CO_2.

HIV-positive donors, ethics statement, and cell isolation
The present study was approved by the Institutional Review Board of the Centre Hospitalier Universitaire Vaudois, and all individuals gave written informed consent. Blood mononuclear cells used in the in vitro functional assay were obtained following leukapheresis performed on eight HIV-positive donors that were chronically infected based on virological and clinical profiles (Vajpayee et al., 2005). Blood mononuclear cells were isolated as previously described (Perreau and Kremer, 2005) and cryopreserved in liquid nitrogen.

Luminex binding assay
The human PD-1 Fc fusion protein (R&D Systems) was conjugated to Bio-Plex magnetic beads (Bio-Rad) according to the manufacturer's protocol and used in a primary screen for anti–PD-1 Ab binding affinity. Ab serial dilutions were incubated with PD-1 Fc-coated beads for 2 h with bound mouse Ab detected using a PE-labeled anti-mouse IgG secondary in a Luminex binding assay. In the competitive binding assay performed with a commercial anti–PD-1 Ab, PD-1 Fc-conjugated Bio-Plex beads were preincubated with one of the novel anti–PD-1 Ab clones. A biotinylated clone EH12.2H7 anti–PD-1 Ab was then added to the beads and incubated for 2 h before staining for the bound commercial Abs with PE-labeled streptavidin. Competitive Ab binding to PD-1 results in a reduction in mean fluorescence intensity relative to biotinylated EH12.2H7 Ab binding in the absence of a competitor Ab. Beads were analyzed on a FLEXMAP 3D or Luminex 100 instrument (Luminex Corporation).

The PD-1–PDL-1 biochemical protein–protein interaction assay was performed by preincubating PD-1 Fc coated Bio-Plex

Fenwick et al.
Enhanced anti–PD-1–mediated immune recovery

Journal of Experimental Medicine
https://doi.org/10.1084/jem.20182359

1536

beads in the presence of 20 nM of anti–PD-1 Ab (clones 137F2, 135C12, and 136B4) or a mouse IgG1 isotype control for 1 h. Duplicate samples of biotinylated PD-L1 Fc protein (R&D Systems) were added in a concentration range from 0.08 to 10 nM to the preformed Ab–PD-1 complex and incubated for a further 4 h before removing unbound PDL-1 and staining beads with PE-labeled streptavidin. In a variation of this assay to identify blocking Abs, PD-1 Fc–coated Bio-Plex beads were preincubated for 1 h with up to 20 nM anti–PD-1 Ab followed by a 4-h incubation with 1.25 nM biotinylated PDL-1 protein, a concentration that gave half-maximal binding to the PD-1–coated beads in the absence of Ab competitor. Bound PDL-1 was stained with PE-labeled streptavidin and measured with the Luminex 100 instrument.

Ab epitope mapping studies

The pReceiver-M67 vector encoding the open reading frame the PDCD1 gene (GeneCopoeia) was used to express human PD-1, and vectors encoding the amino acid substitutions in PD-1 listed in Fig. S4 were generated using the Q5 Site-Directed Mutagenesis Kit (New England Biolabs) according to the manufacturer's protocol. These PD-1 expression vectors together with an enhanced GFP pcDNA3 construct (Addgene) were used to transiently transfect HeLa cells using the FuGENE 6 transfection reagent (Promega). Following a 2-d incubation at 37°C, the adherent HeLa cells were detached from the plates with a stream of PBS and labeled with the Aqua LIVE/DEAD staining kit (Thermo Fisher Scientific). Ab binding to wild-type or mutant forms of PD-1 was performed in parallel by incubating the different transfected cell samples with 2 µg/ml of the indicated mouse anti–PD-1 Ab followed by a PE-labeled F(ab')2-goat anti-mouse IgG secondary Ab. Binding of pembrolizumab to the transiently transfected HeLa cells expressing the different PD-1 constructs was detected using PE-labeled goat anti-human IgG secondary Ab. Flow cytometry analysis of the samples was performed on an LSR II (Becton Dickinson) with Ab binding for the different wild-type and mutant PD-1 constructs evaluated for the live, enhanced GFP–expressing HeLa cells. Flow cytometry histogram results presented are representative of two to four independent experiments.

Ab binding to cell-surface PD-1 and a competitive binding assay

A Jurkat cell line stably transfected to express high levels of human PD-1 (BPS Biosciences) was used to evaluate Ab binding affinity to cell-surface PD-1. These cells were incubated with different Ab concentrations, washed, stained with a PE–labeled anti-mouse or anti-human secondary Ab, and analyzed by flow cytometry. Percent detection of PD-1 positive cells was determined for each Ab concentration and binding affinities were determined with the GraphPad Prism7 software using a non-linear curve-fitting analysis.

Competitive binding between different anti–PD-1 Ab clones to Jurkat PD-1 cells was performed by adding saturating amounts (40 µg/ml) mouse IgG1 competitor Ab (137F2, 135C12, or 136B4) with cells incubated for 30 min followed by 1 µg/ml of the indicated human IgG4 anti–PD-1 Abs. The PE-labeled goat anti-human IgG secondary Ab was used to detect the levels of human anti–PD-1 Abs binding to cell-surface PD-1 in the presence of competitor. Maximal binding to the Jurkat PD-1 cells was equivalent for all human anti–PD-1 Abs, and the positive control in each graph is shown for pembrolizumab staining.

Functional exhaustion CFSE proliferation assay

Cryopreserved blood mononuclear cells from a patient with chronic HIV infection were thawed and resuspended in RPMI medium containing 20% FBS, washed with 37°C PBS, and rested in RPMI medium with 10% FBS overnight. The following morning, cells were washed twice with 37°C PBS and then incubated with 20 µM CFSE (Invitrogen) at 37°C for 7 min in the dark. The staining was quenched with the addition of FBS at a final concentration of 10% and then washed twice with RPMI medium. An aliquot of CFSE-stained blood mononuclear cells was set aside for the negative control samples, and the remaining peripheral blood mononuclear cells were batch stimulated with the addition of the indicated HIV antigenic peptide (GPT) to give a final concentration of 1.11 µg/ml. Peptide-stimulated and nonstimulated cells were then distributed into 48-well plates at 10^6 cells per well in 900 µl. Replicates of 8–10 wells were prepared for each condition tested. Abs tested were prepared in a 10× stock in RPMI + 6% human serum, then 100 µl was added to the appropriate wells to have a final peptide concentration of 1 µg/ml and final Ab concentration of 5 µg/ml unless otherwise indicated. As additional controls, a mouse IgG1 or human IgG4 isotype control Ab at a final concentration of 5 µg/ml was included in most experiments, and one well of cells was stimulated with staphylococcal enterotoxin B as a positive control for the induction of cellular proliferation. All samples within the 48-well plates were then returned to the 37°C, 5% CO_2 incubator for 6 d.

On the sixth day, the cells were harvested from wells and washed with warm PBS, as before. The cells were then labeled with Aqua viability stain and incubated with an Ab cocktail containing anti-CD3 APC Cy7, anti-CD4 PE CF 594, and anti-CD8 Pacific blue. The samples were then analyzed by flow cytometry on the LSR II SORP four-laser (405, 488, 532, and 633 nm) instrument. The five different chronic HIV-infected patients used for the CFSE proliferation assay studies were B08, B09, C10, M34, and M114.

Assessment of cytokine production

Cryopreserved blood mononuclear cells from eight different HIV-infected donors (B08, B09, C10, M34, M114, B02, M24, and M46) were used in studies monitoring cytokine production following Ag-specific stimulations in the presence and absence of anti–PD-1 Abs. The protocol for HIV antigenic peptide stimulations is the same as described above for the proliferation assay with the omission of the CFSE cell staining. Following a 3-d incubation in culture, cell medium supernatants were assessed for levels of INF-γ, TNF-α, IL-2, and IL-10 by Luminex assay using a ProcartaPlex custom human 4-plex kit (Thermo Fisher Scientific) according the manufacturer's protocol with measurements performed on the Luminex 100 instrument.

Fenwick et al.
Enhanced anti–PD-1–mediated immune recovery

Journal of Experimental Medicine
https://doi.org/10.1084/jem.20182359

1537

Purification of hPD1 and the hPD-1–Fab NB01a complex

The expression of hPD-1 33–150 (UniProt Q15116), cloned into pET-24d (kindly provided by Krzysztof M. Zak and Tad A. Holak; Faculty of Biochemistry, Biophysics, and Biotechnology, Jagiellonian University, Krakow, Poland), was induced with 1 mM isopropyl β-D-1-thiogalactopyranoside for 5 h at 37°C in *Escherichia coli* BL21 (DE3) cells, and the protein purification protocol was adapted from Zak et al. (2015). Briefly, induced cells were lysed by sonication with recovery of the inclusion bodies by centrifugation at 20,000 rpm. The inclusion bodies were resuspended in 50 mM Tris, pH 8.0, 6 M guanidine hydrochloride, 200 mM NaCl, and 20 mM β-mercaptoethanol before drop-wise dilution into ice-cold refolding buffer containing 0.1 M Tris-HCl, pH 8.0, 0.4 M L-arginine, 2 mM EDTA, 2 mM reduced glutathione, and 0.2 mM oxidized glutathione. Overnight refolding at 4°C was followed by dialysis and sample loading onto HiTrap Q HP and HiTrap SP FF columns (GE Healthcare). The flow through was concentrated and run in a Superdex 200 10/300 size-exclusion chromatography (GE Healthcare) column.

(Fab)$_2$ and Fab species were generated by digestion of the NB01a IgG4 with the FabRICATOR protease at 4°C overnight according to the manufacturer's protocol with the Fc domain removed using a Protein A affinity column (Thermo Fisher Scientific). (Fab)$_2$ were reduced to Fab with the addition of 2 mM dithiothreitol. Complexes were assembled by mixing hPD-1 with the Fab or reduced (Fab)$_2$ NB01a species in a 1.5:1 molar ratio. After 45 min of incubation at room temperature, the complexes were loaded onto a size-exclusion chromatography Superdex 200 10/300 column equilibrated with 10 mM Tris HCl, 70 mM NaCl, and 2 mM dithiothreitol. Fractions in which the complex eluted were concentrated down to 4.3 mg/ml.

Data collection, processing, and refinement of the x-ray structure

X-ray data were collected at the European Synchrotron Radiation Facility (ESRF), Grenoble, France, at the ID29 beamline (Table S1). Data were collected at a wavelength of 0.97625 Å with a crystal to detector distance of 398.81 mm and a 0.15° rotation of the crystal to complete a total rotation of 150°. The data were processed with XDS (Kabsch, 2010) using the resolution range 65.49–2.2 Å. The structure of the complex was solved by molecular replacement in Phaser MR (McCoy et al., 2007; Read and McCoy, 2011; Z-score 14.9) using hPD-1 in complex with hPD-L1 (PDB accession no. 4ZQK) and a model built in Phenix using coordinates from Fab BL3-6 (PDB accession no. 4Q9Q; Huang et al., 2014), which exhibits high sequence homology with Fab NB01a (90% and 73% with the heavy and light chains, respectively) as search models. The model of the complex was refined in Phenix (Adams et al., 2010) and Refmac5 (Murshudov et al., 2011) and adjusted manually in Coot (Emsley and Cowtan, 2004) to values of $R_{factor} = 0.2120$ and $R_{free} = 0.2760$. The software Contact, part of the CCP4 suite like Phaser MR and REFMAC5 (Winn et al., 2011) and PDBePISA (Krissinel and Henrick, 2007), were used to identify contacts in the binding interface. Structure representations were prepared using CCP4mg (McNicholas et al., 2011). The data for this study are available under PDB accession no. 6HIG.

Modeling of the hPD-1–136B4Fv interaction

The model of 136B4 was built using Phenix software and the aligned sequences of 136B4 and the Fv from PDB file 1DZB (Aÿ et al., 2000), which shares 63% identity with 136B4. In addition to the high sequence identity, this PDB file was selected because it comprises an Fv, which is expected to adopt a similar fold to 136B4. Subsequently, models for the light and heavy chains were searched on the PDB to model the CDRs. The heavy and light chains from PDB files 1MVU and 4M61 (Stanfield and Eilat, 2014) share 79% and 96% of identity with those from 136B4, respectively, and the length of the CDR is comparable. The CDR segments were built into the model provided by Phenix software using Coot.

Phosphoprotein signaling by flow cytometry

Blood mononuclear cells from a viremic HIV-positive donor were incubated with 20 µg/ml of pembrolizumab, NB01b, or IgG4 isotype control for 30 min at 37°C. PDL-1 Fc fusion protein was then added to the indicated test conditions at 20 µg/ml for an additional 30 min. For all conditions except the IgG4 control, anti-CD3/CD28 Ab stimulation was performed at 5 µg/ml of each Ab and cross-linked with an anti-mouse secondary Ab at 50 µg/ml to initiate T cell activation. Cells were incubated at 37°C for various time points (1, 5, and 15 min) and fixed immediately with 2% formaldehyde in PBS at 37°C for 10 min to stop the reaction. Blood mononuclear cells were washed and stained for CD3, CD4, CD8, and CD45RA T cell surface markers at room temperature for 20 min. Following cell permeabilization in chilled 70% methanol for 30 min, intracellular staining with various phosphoproteins was performed. The stained cells were washed and fixed once more in 2% formaldehyde in PBS before FACS acquisition. The percentage of positive phosphoproteins was determined at the different time points following stimulation by applying a global positive gate using the time 0 sample for each experiment as reference.

Calcium flux

Blood mononuclear cells were washed in PBS and incubated with 1 µM of Fluo-4 AM for 15 min at room temperature. Cells were then washed again and incubated with an anti-CD4/CD8 Ab cocktail for T cell markers. Blood mononuclear cells were washed once more and resuspended in RPMI medium. NB01b, pembrolizumab, and/or nivolumab anti–PD-1 Abs were incubated at 10 µg/ml for 30 min at 37°C and PD-L1 protein was incubated at 5 µg/ml for an additional 30 min before the samples were stimulated with the same anti-CD3/CD28 Ab protocol described above and directly analyzed by FACS acquisition. Calcium flux from TCR stimulation was measured in real time for 10 min before ending the reaction with the addition of 2 mM EDTA, which was acquired for a further 1 min.

Immunoprecipitation of the cellular PD-1 protein complex

Immunoprecipitation studies used Dynabeads M-450 Epoxy beads (Thermo Fisher Scientific) covalently coupled with either anti–PD-1 or IgG4 control Abs according to the manufacturer's protocol. For each condition, 10 million Jurkat cells stably expressing PD-1 (BPS Bioscience) were either left

unstimulated or stimulated with biotinylated anti-CD3 (5 µg/ml; OKT3; eBioscience) and anti-CD28 (5 µg/ml; CD28.2; eBioscience) then aggregated with the addition of 50 µg/ml of avidin (Invitrogen). Ab-coated beads were added directly and cells were incubated at 37°C for 10 min. Cell membranes where then lysed with ice cold PBS containing 1% Triton X-100, protease inhibitor cocktail (Complete; Roche) and a phosphatase inhibitor cocktail followed by a 15-min incubation on ice with frequent mixing. Magnetic beads were attracted to the side of each tube with a magnet and washed three times with cell lysis buffer and then once with lysis buffer without detergent. Immune complexes analyzed by Western blot had proteins separated on a NuPAGE 10% Bis-Tris gel (Invitrogen) and then transferred onto nitrocellulose (Bio-Rad). Immunoblotting was performed by staining with the primary Ab overnight at 4°C followed by washing steps and then incubation with the HRP-conjugated secondary Ab and detection with the Pierce ECL Western blotting substrate (Thermo Fisher Scientific) in accordance with the manufacturer's protocol. Blots were imaged with the Fusion FX Vilber Lurmat camera (Witec), and the density of individual bands was evaluated using ImageJ software.

Jurkat PD-1 NFAT and NF-κB reporter assays

The Jurkat PD-1 NFAT reporter assay was performed according the manufactures protocol with minor modifications (BPS Bioscience). 2 d before performing the assay, Jurkat PD-1 NFAT cells were transiently transfected with the NanoLuc reporter vector with an NF-κB response element (Promega) using the Fugene 6 transfection reagent (Promega). Preparation of the activator cells involved transient cotransfected of 293T cells with the TCR activator and PDL-1 expression vectors using the Fugene 6 transfection reagent. The following day, cells were resuspended and seeded at 60–70% confluence in wells of a 96-well plate and then incubated for 5 h to allow cell adherence. The NanoLuc transfected Jurkat PD-1 NFAT reporter cells were added at 100,000 cells per well in the absence of presence of the indicated Abs. The NFAT and NF-κB activation was measured 18 h later using the Nano-Glo Dual-luciferase Reporter assay system (Promega) on the Synergy H1 Hybrid Multi-Mode Microplate Reader (BioTek Instruments).

Mouse tumor model

The in vivo tumor model studies using PD-1 HuGEMM mice (background: C57BL/6) were performed at CrownBio (Taicang, China) in three separate MC38 studies and one B16F10 tumor study. Each mouse was inoculated subcutaneously at the right hind flank with 10^6 MC38 cells or 10^5 B16F10 cells. Mice with successfully engrafted tumors of the desired sized were enrolled in the studies with 10 mice per arm with mean tumor volumes of 82, 84, and 85 mm³ for the first, second, and third MC38 tumor study, respectively. Mice enrolled for the B16F10 study had mean tumor volumes of 65.1 mm³ for the 10 mice per arm of the study. Mice were administered the indicated Abs at a concentration of 0.9 to 1.0 mg/ml in PBS or a sterile PBS vehicle control at twice weekly intervals over the course of the study. All in vivo therapies used a total dose of 10 mg/kg Ab apart from the

combination therapy arm of the B16F10 study, where 10 mg/kg of pembrolizumab and NB01b were administered. Tumor volumes were measured twice weekly in two dimensions using a caliper, and the volume was expressed in cubic millimeters using the formula $V = 0.5\, a \times b^2$, where a and b are the long and short diameters of the tumor, respectively. Body weight was also measured twice weekly. Mice that controlled MC38 tumor growth had a decrease in tumor volume at the end of the study relative to the start, just before initiating Ab therapy. The protocol and any amendments or procedures involving the care and use of animals in this study were reviewed and approved by the Institutional Animal Care and Use Committee of CrownBio before conduct. During the study, the care and use of animals was conducted in accordance with the regulations of the Association for Assessment and Accreditation of Laboratory Animal Care.

Statistical analyses

Statistical significance (P values) between two sample conditions in the in vitro functional assay was obtained using two-tailed unpaired t tests with a Welch correction to account for samples with nonequivalent standard deviations. In the mouse study, a mixed-effects linear model, modeling the volume (after cubic-root transformation) as a function of group, time, and their interaction, was used to test whether the combination therapy had lower mean volume over time than any single therapy. Our model allows for a group-specific slope, taking into account the correlation within mice across time (due to the repeated measurements) and using a mice-specific random effect, which is common for such studies (Galecki and Burzykowski, 2013). The cubic-root transformation was used to stabilize the variance and make the data more normally distributed. It is also a natural transformation for volume measurements as the scale is easily interpretable. Since the original unit is a volume expressed in cubic millimeters, the transformed unit is a length expressed in millimeters. The cube-root transformation is often used to model volume data (Matthews et al., 1990; Gallegos et al., 1996; Mandonnet et al., 2003). Using our model, we tested the null hypothesis that the slope of the combination therapy is equal to the slope of the anti–PD-1 monotherapies alone versus the alternative that the slope is smaller using a two-sided test. In our model, the slope can be interpreted as the rate of increase of the mean tumor diameter over time.

Online supplemental material

Fig. S1 shows the enhanced proliferation of Ag-specific exhausted CD8 T cells in the presence of a panel of prioritized anti–PD-1 Abs. Fig. S2 shows four separate experiments where blocking and nonblocking anti–PD-1 Ab combinations synergize in recovering the proliferation of exhausted Ag-specific CD8 T cells. Fig. S3 shows a PD-1 sequence map of the mutations used for Ab epitope mapping and the sequence alignment of PD-1 from different species. Fig. S4 shows the PD-1–PDL-1–mediated suppression in phospho-signaling following stimulation of exhausted T cells and the relief of this suppression mediated by anti–PD-1 Abs. Table S1 shows the x-ray data statistics for the hPD-1–NB01a Fab complex.

Fenwick et al.
Enhanced anti–PD-1–mediated immune recovery

Journal of Experimental Medicine   1539
https://doi.org/10.1084/jem.20182359

Acknowledgments

References

Adams, P.D., P.V. Afonine, G. Bunkóczi, V.B. Chen, I.W. Davis, N. Echols, J.J. Headd, L.W. Hung, G.J. Kapral, R.W. Grosse-Kunstleve, et al. 2010. PHENIX: a comprehensive Python-based system for macromolecular structure solution. *Acta Crystallogr. D Biol. Crystallogr.* 66:213–221. https://doi.org/10.1107/S0907444909052925

Aÿ, J., T. Keitel, G. Küttner, H. Wessner, C. Scholz, M. Hahn, and W. Höhne. 2000. Crystal structure of a phage library-derived single-chain Fv fragment complexed with turkey egg-white lysozyme at 2.0 A resolution. *J. Mol. Biol.* 301:239–246. https://doi.org/10.1006/jmbi.2000.3971

Baitsch, L., P. Baumgaertner, E. Devêvre, S.K. Raghav, A. Legat, L. Barba, S. Wieckowski, H. Bouzourene, B. Deplancke, P. Romero, et al. 2011. Exhaustion of tumor-specific CD8⁺ T cells in metastases from melanoma patients. *J. Clin. Invest.* 121:2350–2360. https://doi.org/10.1172/JCI46102

Barber, D.L., E.J. Wherry, D. Masopust, B. Zhu, J.P. Allison, A.H. Sharpe, G.J. Freeman, and R. Ahmed. 2006. Restoring function in exhausted CD8 T cells during chronic viral infection. *Nature.* 439:682–687. https://doi.org/10.1038/nature04444

Callahan, M.K., M.A. Postow, and J.D. Wolchok. 2016. Targeting T Cell Co-receptors for Cancer Therapy. *Immunity.* 44:1069–1078. https://doi.org/10.1016/j.immuni.2016.04.023

Carbognin, L., S. Pilotto, M. Milella, V. Vaccaro, M. Brunelli, A. Caliò, F. Cuppone, I. Sperduti, D. Giannarelli, M. Chilosi, et al. 2015. Differential Activity of Nivolumab, Pembrolizumab and MPDL3280A according to

the Tumor Expression of Programmed Death-Ligand-1 (PD-L1): Sensitivity Analysis of Trials in Melanoma, Lung and Genitourinary Cancers. *PLoS One.* 10:e0130142. https://doi.org/10.1371/journal.pone.0130142

Chemnitz, J.M., R.V. Parry, K.E. Nichols, C.H. June, and J.L. Riley. 2004. SHP-1 and SHP-2 associate with immunoreceptor tyrosine-based switch motif of programmed death 1 upon primary human T cell stimulation, but only receptor ligation prevents T cell activation. *J. Immunol.* 173:945–954. https://doi.org/10.4049/jimmunol.173.2.945

Chen, S., L.F. Lee, T.S. Fisher, B. Jessen, M. Elliott, W. Evering, K. Logronio, G.H. Tu, K. Tsaparikos, X. Li, et al. 2015. Combination of 4-1BB agonist and PD-1 antagonist promotes antitumor effector/memory CD8 T cells in a poorly immunogenic tumor model. *Cancer Immunol. Res.* 3:149–160. https://doi.org/10.1158/2326-6066.CIR-14-0118

Day, C.L., D.E. Kaufmann, P. Kiepiela, J.A. Brown, E.S. Moodley, S. Reddy, E.W. Mackey, J.D. Miller, A.J. Leslie, C. DePierres, et al. 2006. PD-1 expression on HIV-specific T cells is associated with T-cell exhaustion and disease progression. *Nature.* 443:350–354. https://doi.org/10.1038/nature05115

Emsley, P., and K. Cowtan. 2004. Coot: model-building tools for molecular graphics. *Acta Crystallogr. D Biol. Crystallogr.* 60:2126–2132. https://doi.org/10.1107/S0907444904019158

Galecki, A., and T. Burzykowski. 2013. *Linear Mixed-Effects Models Using R: A Step-by-Step Approach.* Springer, New York. 542 pp. https://doi.org/10.1007/978-1-4614-3900-4

Gallegos, A., J.R. Gasdaska, C.W. Taylor, G.D. Paine-Murrieta, D. Goodman, P.Y. Gasdaska, M. Berggren, M.M. Briehl, and G. Powis. 1996. Transfection with human thioredoxin increases cell proliferation and a dominant-negative mutant thioredoxin reverses the transformed phenotype of human breast cancer cells. *Cancer Res.* 56:5765–5770.

Gandini, S., D. Massi, and M. Mandalà. 2016. PD-L1 expression in cancer patients receiving anti PD-1/PD-L1 antibodies: A systematic review and meta-analysis. *Crit. Rev. Oncol. Hematol.* 100:88–98. https://doi.org/10.1016/j.critrevonc.2016.02.001

Hamid, O., C. Robert, A. Daud, F.S. Hodi, W.J. Hwu, R. Kefford, J.D. Wolchok, P. Hersey, R.W. Joseph, J.S. Weber, et al. 2013. Safety and tumor responses with lambrolizumab (anti-PD-1) in melanoma. *N. Engl. J. Med.* 369:134–144. https://doi.org/10.1056/NEJMoa1305133

Huang, A., D. Peng, H. Guo, Y. Ben, X. Zuo, F. Wu, X. Yang, F. Teng, Z. Li, X. Qian, and F.X. Qin. 2017. A human programmed death-ligand 1-expressing mouse tumor model for evaluating the therapeutic efficacy of anti-human PD-L1 antibodies. *Sci. Rep.* 7:42687. https://doi.org/10.1038/srep42687

Huang, H., N.B. Suslov, N.S. Li, S.A. Shelke, M.E. Evans, Y. Koldobskaya, P.A. Rice, and J.A. Piccirilli. 2014. A G-quadruplex-containing RNA activates fluorescence in a GFP-like fluorophore. *Nat. Chem. Biol.* 10:686–691. https://doi.org/10.1038/nchembio.1561

Hui, E., J. Cheung, J. Zhu, X. Su, M.J. Taylor, H.A. Wallweber, D.K. Sasmal, J. Huang, J.M. Kim, I. Mellman, and R.D. Vale. 2017. T cell costimulatory receptor CD28 is a primary target for PD-1-mediated inhibition. *Science.* 355:1428–1433. https://doi.org/10.1126/science.aaf1292

Kabsch, W. 2010. Xds. *Acta Crystallogr. D Biol. Crystallogr.* 66:125–132. https://doi.org/10.1107/S0907444909047337

Kamphorst, A.O., A. Wieland, T. Nasti, S. Yang, R. Zhang, D.L. Barber, B.T. Konieczny, C.Z. Daugherty, L. Koenig, K. Yu, et al. 2017. Rescue of exhausted CD8 T cells by PD-1-targeted therapies is CD28-dependent. *Science.* 355:1423–1427. https://doi.org/10.1126/science.aaf0683

Kokolus, K.M., Y. Zhang, J.M. Sivik, C. Schmeck, J. Zhu, E.A. Repasky, J.J. Drabick, and T.D. Schell. 2017. Beta blocker use correlates with better overall survival in metastatic melanoma patients and improves the efficacy of immunotherapies in mice. *OncoImmunology.* 7:e1405205. https://doi.org/10.1080/2162402X.2017.1405205

Krissinel, E., and K. Henrick. 2007. Inference of macromolecular assemblies from crystalline state. *J. Mol. Biol.* 372:774–797. https://doi.org/10.1016/j.jmb.2007.05.022

Kuzu, O.F., F.D. Nguyen, M.A. Noory, and A. Sharma. 2015. Current State of Animal (Mouse) Modeling in Melanoma Research. *Cancer Growth Metastasis.* 8(Suppl 1):81–94.

Larkin, J., V. Chiarion-Sileni, R. Gonzalez, J.J. Grob, C.L. Cowey, C.D. Lao, D. Schadendorf, R. Dummer, M. Smylie, P. Rutkowski, et al. 2015. Combined Nivolumab and Ipilimumab or Monotherapy in Untreated Melanoma. *N. Engl. J. Med.* 373:23–34. https://doi.org/10.1056/NEJMoa1504030

Lázár-Molnár, E., Q. Yan, E. Cao, U. Ramagopal, S.G. Nathenson, and S.C. Almo. 2008. Crystal structure of the complex between programmed death-1 (PD-1) and its ligand PD-L2. *Proc. Natl. Acad. Sci. USA.* 105:10483–10488. https://doi.org/10.1073/pnas.0804453105

Fenwick et al.
Enhanced anti–PD-1–mediated immune recovery

Journal of Experimental Medicine
https://doi.org/10.1084/jem.20182359

1540

Lee, J.Y., H.T. Lee, W. Shin, J. Chae, J. Choi, S.H. Kim, H. Lim, T. Won Heo, K.Y. Park, Y.J. Lee, et al. 2016. Structural basis of checkpoint blockade by monoclonal antibodies in cancer immunotherapy. *Nat. Commun.* 7: 13354. https://doi.org/10.1038/ncomms13354

Lin, D.Y., Y. Tanaka, M. Iwasaki, A.G. Gittis, H.P. Su, B. Mikami, T. Okazaki, T. Honjo, N. Minato, and D.N. Garboczi. 2008. The PD-1/PD-L1 complex resembles the antigen-binding Fv domains of antibodies and T cell receptors. *Proc. Natl. Acad. Sci. USA.* 105:3011–3016. https://doi.org/10.1073/pnas.0712278105

Lute, K.D., K.F. May Jr., P. Lu, H. Zhang, E. Kocak, B. Mosinger, C. Wolford, G. Phillips, M.A. Caligiuri, P. Zheng, and Y. Liu. 2005. Human CTLA4 knock-in mice unravel the quantitative link between tumor immunity and autoimmunity induced by anti-CTLA-4 antibodies. *Blood.* 106:3127–3133. https://doi.org/10.1182/blood-2005-06-2298

Mandonnet, E., J.Y. Delattre, M.L. Tanguy, K.R. Swanson, A.F. Carpentier, H. Duffau, P. Cornu, R. Van Effenterre, E.C. Alvord Jr., and L. Capelle. 2003. Continuous growth of mean tumor diameter in a subset of grade II gliomas. *Ann. Neurol.* 53:524–528. https://doi.org/10.1002/ana.10528

Matthews, J.N., D.G. Altman, M.J. Campbell, and P. Royston. 1990. Analysis of serial measurements in medical research. *BMJ.* 300:230–235. https://doi.org/10.1136/bmj.300.6719.230

McCoy, A.J., R.W. Grosse-Kunstleve, P.D. Adams, M.D. Winn, L.C. Storoni, and R.J. Read. 2007. Phaser crystallographic software. *J. Appl. Cryst.* 40: 658–674. https://doi.org/10.1107/S0021889807021206

McNicholas, S., E. Potterton, K.S. Wilson, and M.E. Noble. 2011. Presenting your structures: the CCP4mg molecular-graphics software. *Acta Crystallogr. D Biol. Crystallogr.* 67:386–394. https://doi.org/10.1107/S0907444911007281

Mellman, I., G. Coukos, and G. Dranoff. 2011. Cancer immunotherapy comes of age. *Nature.* 480:480–489. https://doi.org/10.1038/nature10673

Murshudov, G.N., P. Skubák, A.A. Lebedev, N.S. Pannu, R.A. Steiner, R.A. Nicholls, M.D. Winn, F. Long, and A.A. Vagin. 2011. REFMAC5 for the refinement of macromolecular crystal structures. *Acta Crystallogr. D Biol. Crystallogr.* 67:355–367. https://doi.org/10.1107/S0907444911001314

Pantaleo, G., and C. Fenwick. 2016. Immunological reagents. MabQuest SA patent application WO/2016/020856 A2, filed August 5, 2015, and published February 11, 2016.

Parry, R.V., J.M. Chemnitz, K.A. Frauwirth, A.R. Lanfranco, I. Braunstein, S.V. Kobayashi, P.S. Linsley, C.B. Thompson, and J.L. Riley. 2005. CTLA-4 and PD-1 receptors inhibit T-cell activation by distinct mechanisms. *Mol. Cell. Biol.* 25:9543–9553. https://doi.org/10.1128/MCB.25.21.9543-9553.2005

Patsoukis, N., J. Brown, V. Petkova, F. Liu, L. Li, and V.A. Boussiotis. 2012. Selective effects of PD-1 on Akt and Ras pathways regulate molecular components of the cell cycle and inhibit T cell proliferation. *Sci. Signal.* 5:ra46. https://doi.org/10.1126/scisignal.2002796

Patsoukis, N., L. Li, D. Sari, V. Petkova, and V.A. Boussiotis. 2013. PD-1 increases PTEN phosphatase activity while decreasing PTEN protein stability by inhibiting casein kinase 2. *Mol. Cell. Biol.* 33:3091–3098. https://doi.org/10.1128/MCB.00319-13

Pauken, K.E., and E.J. Wherry. 2015. Overcoming T cell exhaustion in infection and cancer. *Trends Immunol.* 36:265–276. https://doi.org/10.1016/j.it.2015.02.008

Perreau, M., and E.J. Kremer. 2005. Frequency, proliferation, and activation of human memory T cells induced by a nonhuman adenovirus. *J. Virol.* 79:14595–14605. https://doi.org/10.1128/JVI.79.23.14595-14605.2005

Read, R.J., and A.J. McCoy. 2011. Using SAD data in Phaser. *Acta Crystallogr. D Biol. Crystallogr.* 67:338–344. https://doi.org/10.1107/S0907444910051371

Rizvi, N.A., J. Mazières, D. Planchard, T.E. Stinchcombe, G.K. Dy, S.J. Antonia, L. Horn, H. Lena, E. Minenza, B. Mennecier, et al. 2015. Activity and safety of nivolumab, an anti-PD-1 immune checkpoint inhibitor, for patients with advanced, refractory squamous non-small-cell lung cancer (CheckMate 063): a phase 2, single-arm trial. *Lancet Oncol.* 16: 257–265. https://doi.org/10.1016/S1470-2045(15)70054-9

Sharma, P., and J.P. Allison. 2015. The future of immune checkpoint therapy. *Science.* 348:56–61. https://doi.org/10.1126/science.aaa8172

Sheppard, K.A., L.J. Fitz, J.M. Lee, C. Benander, J.A. George, J. Wooters, Y. Qiu, J.M. Jussif, L.L. Carter, C.R. Wood, and D. Chaudhary. 2004. PD-1 inhibits T-cell receptor induced phosphorylation of the ZAP70/CD3zeta signalosome and downstream signaling to PKCtheta. *FEBS Lett.* 574: 37–41. https://doi.org/10.1016/j.febslet.2004.07.083

Stanfield, R.L., and D. Eilat. 2014. Crystal structure determination of anti-DNA Fab A52. *Proteins.* 82:1674–1678. https://doi.org/10.1002/prot.24514

Topalian, S.L., F.S. Hodi, J.R. Brahmer, S.N. Gettinger, D.C. Smith, D.F. McDermott, J.D. Powderly, R.D. Carvajal, J.A. Sosman, M.B. Atkins, et al. 2012. Safety, activity, and immune correlates of anti-PD-1 antibody in cancer. *N. Engl. J. Med.* 366:2443–2454. https://doi.org/10.1056/NEJMoa1200690

Trautmann, L., L. Janbazian, N. Chomont, E.A. Said, S. Gimmig, B. Bessette, M.R. Boulassel, E. Delwart, H. Sepulveda, R.S. Balderas, et al. 2006. Upregulation of PD-1 expression on HIV-specific CD8+ T cells leads to reversible immune dysfunction. *Nat. Med.* 12:1198–1202. https://doi.org/10.1038/nm1482

Tumeh, P.C., C.L. Harview, J.H. Yearley, I.P. Shintaku, E.J. Taylor, L. Robert, B. Chmielowski, M. Spasic, G. Henry, V. Ciobanu, et al. 2014. PD-1 blockade induces responses by inhibiting adaptive immune resistance. *Nature.* 515:568–571. https://doi.org/10.1038/nature13954

Vajpayee, M., S. Kaushik, V. Sreenivas, N. Wig, and P. Seth. 2005. CDC staging based on absolute CD4 count and CD4 percentage in an HIV-1-infected Indian population: treatment implications. *Clin. Exp. Immunol.* 141:485–490. https://doi.org/10.1111/j.1365-2249.2005.02857.x

Wherry, E.J., and M. Kurachi. 2015. Molecular and cellular insights into T cell exhaustion. *Nat. Rev. Immunol.* 15:486–499. https://doi.org/10.1038/nri3862

Winn, M.D., C.C. Ballard, K.D. Cowtan, E.J. Dodson, P. Emsley, P.R. Evans, R.M. Keegan, E.B. Krissinel, A.G. Leslie, A. McCoy, et al. 2011. Overview of the CCP4 suite and current developments. *Acta Crystallogr. D Biol. Crystallogr.* 67:235–242. https://doi.org/10.1107/S0907444910045749

Woods, D.M., A.L. Sodré, A. Villagra, A. Sarnaik, E.M. Sotomayor, and J. Weber. 2015. HDAC Inhibition Upregulates PD-1 Ligands in Melanoma and Augments Immunotherapy with PD-1 Blockade. *Cancer Immunol. Res.* 3:1375–1385. https://doi.org/10.1158/2326-6066.CIR-15-0077-T

Yokosuka, T., M. Takamatsu, W. Kobayashi-Imanishi, A. Hashimoto-Tane, M. Azuma, and T. Saito. 2012. Programmed cell death 1 forms negative costimulatory microclusters that directly inhibit T cell receptor signaling by recruiting phosphatase SHP2. *J. Exp. Med.* 209:1201–1217. https://doi.org/10.1084/jem.20112741

Zak, K.M., R. Kitel, S. Przetocka, P. Golik, K. Guzik, B. Musielak, A. Dömling, G. Dubin, and T.A. Holak. 2015. Structure of the Complex of Human Programmed Death 1, PD-1, and Its Ligand PD-L1. *Structure.* 23: 2341–2348. https://doi.org/10.1016/j.str.2015.09.010

Zamarin, D., J.M. Ricca, S. Sadekova, A. Oseledchyk, Y. Yu, W.M. Blumenschein, J. Wong, M. Gigoux, T. Merghoub, and J.D. Wolchok. 2018. PD-L1 in tumor microenvironment mediates resistance to oncolytic immunotherapy. *J. Clin. Invest.* 128:5184. https://doi.org/10.1172/JCI125039

Zhang, J.Y., Z. Zhang, X. Wang, J.L. Fu, J. Yao, Y. Jiao, L. Chen, H. Zhang, J. Wei, L. Jin, et al. 2007. PD-1 up-regulation is correlated with HIV-specific memory CD8+ T-cell exhaustion in typical progressors but not in long-term nonprogressors. *Blood.* 109:4671–4678. https://doi.org/10.1182/blood-2006-09-044826